AN ITERATIVE SUBSTRUCTURING ALGORITHM FOR TWO-DIMENSIONAL PROBLEMS IN H(CURL) TR2010-936

CLARK R. DOHRMANN* AND OLOF B. WIDLUND†

December 13, 2010

Abstract. A domain decomposition algorithm, similar to classical iterative substructuring algorithms, is presented for two-dimensional problems in the space $H_0(\mathrm{curl};\Omega)$. It is defined in terms of a coarse space and local subspaces associated with individual edges of the subdomains into which the domain of the problem has been subdivided. The algorithm differs from others in three basic respects. First, it can be implemented in an algebraic manner that does not require access to individual subdomain matrices or a coarse discretization of the domain; this is in contrast to algorithms of the BDDC, FETI–DP, and classical two–level overlapping Schwarz families. Second, favorable condition number bounds can be established over a broader range of subdomain material properties than in previous studies. Third, we are able to develop theory for quite irregular subdomains and bounds for the condition number of our preconditioned conjugate gradient algorithm, which depend only on a few geometric parameters.

The coarse space for the algorithm is based on simple energy minimization concepts, and its dimension equals the number of subdomain edges. Numerical results are presented which confirm the theory and demonstrate the usefulness of the algorithm for a variety of mesh decompositions and distributions of material properties.

Key words. domain decomposition, iterative substructuring, H(curl), Maxwell's equations, preconditioners, irregular subdomain boundaries, discontinuous coefficients

AMS subject classifications. 35Q60, 65F10, 65N30, 65N55

1. Introduction. In this paper, we introduce and analyze a domain decomposition algorithm for two-dimensional (2D) problems in the space $H_0(\mathrm{curl};\Omega)$. The core issues of the present study concern an energy-minimizing coarse space in 2D for edge finite element approximations of the variational problem: Find $\boldsymbol{u} \in H_0(\mathrm{curl};\Omega)$ such that

$$a_\Omega(\boldsymbol{u},\boldsymbol{v}) = (\boldsymbol{f},\boldsymbol{v})_\Omega \quad \forall \boldsymbol{v} \in H_0(\mathrm{curl};\Omega),$$

where

$$a_\Omega(\boldsymbol{u},\boldsymbol{v}) := \int_\Omega [(\alpha \nabla\times\boldsymbol{u}\cdot\nabla\times\boldsymbol{v}) + (B\boldsymbol{u}\cdot\boldsymbol{v})]\,dx, \quad (\boldsymbol{f},\boldsymbol{v})_\Omega = \int_\Omega \boldsymbol{f}\cdot\boldsymbol{v}\,dx.$$

This variational problem originates, for example, from implicit time integration of the eddy current model of Maxwell's equations,where α is the reciprocal of the magnetic permeability and B is proportional to the electrical conductivity divided by the time step; we note that this is the same problem considered in, e.g., [2, 11, 21]. The norm of $\boldsymbol{u} \in H(\mathrm{curl};\Omega)$, for a domain with diameter 1, is given by $a_\Omega(\boldsymbol{u},\boldsymbol{u})^{1/2}$ with $\alpha = 1$

*Analytical Structural Dynamics Department, Sandia National Laboratories, Albuquerque, New Mexico, 87185 crdohrm@sandia.gov. Sandia is a multiprogram laboratory operated by Sandia Corporation, a Lockheed Martin Company, for the United States Department of Energy's National Nuclear Security Administration under Contract DE-AC04-94-AL85000.

†Courant Institute, 251 Mercer Street, New York NY 10012, USA widlund@cims.nyu.edu, http://www.cs.nyu.edu/cs/faculty/widlund. This work was supported in part by the U.S. Department of Energy under contracts DE-FG02-06ER25718 and in part by National Science Foundation Grant DMS-0914954. Part of the work of this author was also supported by the Institute of Mathematical Sciences and the Department of Mathematics of the Chinese University of Hong Kong.

and $B = I$; the elements of $H_0(\text{curl})$ have vanishing tangential components on $\partial\Omega$. We could equally well consider cases where this boundary condition is imposed only on one or several subdomain edges, which form part of $\partial\Omega$ and which are defined in the beginning of the next section. Generally, $\alpha \geq 0$ and B is a 2x2 positive definite symmetric matrix. We will assume that α is a constant $\alpha_i \geq 0$ in each of the subdomains Ω_i. Likewise, we replace B by the scalar constant $\beta_i > 0$ for each of the Ω_i. Our results could be presented in a form which accommodates properties which are not constant or isotropic in each subdomain, but we avoid this generalization for purposes of clarity.

Many theoretical studies on domain decomposition methods are carried out in the Schwarz framework; cf. [24, Subsect. 2.2]. Let κ denote the condition number of the additive Schwarz operator for some selection of spaces that define a particular Schwarz algorithm. For α_i and β_i constant in each subdomain Ω_i, the estimate

$$\kappa \leq C \max_i (1 + H_i^2 \beta_i / \alpha_i)(1 + \log(H_i/h_i))^2 \tag{1.1}$$

is given in [25] for an iterative substructuring method in 2D with a coarse space based on standard coarse triangular edge finite elements. Here, and in what follows, C is a constant independent of the number of subdomains and the mesh size. Closely related results appear in [19] for Neumann-Neumann methods, in [22] and [17] for a one-level FETI method, and in [23] for a FETI-DP method. The estimate in (1.1) is clearly unfavorable for large values of $H_i^2 \beta_i / \alpha_i$; we will refer to this case as *mass-dominated* while in a *curl-dominated* case this factor is bounded from above. A factor of $H_i^2 \beta_i / \alpha_i$ also appears in condition number estimates for more recent results on a FETI-DP algorithm in 3D [21].

We avoid this factor in the present analysis by using a nonstandard coarse space based on energy minimization concepts rather than one based on conventional edge finite elements. We note that we have also studied energy-minimizing coarse spaces recently for almost incompressible elasticity problems in [6, 7].

The estimate

$$\kappa \leq C(1 + \log(H/h))^3$$

appears in [12] for a 3D iterative substructuring method. The authors were unable to conclude whether this condition number bound is independent of jumps in coefficients between subdomains. In addition, the coarse space dimension is relatively large, being proportional to the number of fine edges which comprise all subdomain edges.

The estimate

$$\kappa \leq C(1 + (H/\delta))^2 \tag{1.2}$$

is given in [20] for an overlapping Schwarz algorithm in 3D. In (1.2), H/δ is the largest ratio of subdomain diameter to overlap length parameter for all subdomains. The coarse space in [20] consists of standard edge finite element functions for coarse tetrahedral elements. For purposes of analysis, the domain was assumed convex and constant material properties were considered. In comparison, our theory allows for a much broader range of material properties and subdomain geometries.

We are unaware of any existing domain decomposition theory in either 2D or 3D that gives a favorable condition number bound independent of all possible jumps in material properties between subdomains. Moreover, current domain decomposition theory for this class of problems is restricted to regular-shaped subdomains. We

address both these issues for 2D problems in this study; this work builds on earlier work for regular elliptic problems and linear elasticity; see [5, 15, 6]. Our algorithms are well-defined and straightforward to implement in all cases and we are able to obtain results for quite general subdomains which do not even need to be uniformly Lipschitz. Moreover, we have also observed, in numerical experiments, that the performance of the algorithm is not diminished significantly in many cases when mesh partitioning tools are used for the decomposition. Earlier numerical results for an overlapping Schwarz method based on a closely related coarse space appear in [4].

The organization of the paper is as follows. To begin, the coarse space for our algorithm and notation are introduced in Section 2. Supporting technical tools for the analysis are then provided in Section 3. The analysis of the coarse interpolant and local decomposition appear in Sections 4 and 5. Our algorithm, its analysis, and some implementation details are presented in Section 6, while numerical results, which confirm the theory and demonstrate the utility of the algorithm, are given in Section 7.

2. A coarse space and notation. We assume that the domain Ω is decomposed into N non-overlapping subdomains $\Omega_1, \ldots, \Omega_N$, each the union of elements of the triangulation of Ω. Each Ω_i is simply connected and has a connected boundary $\partial\Omega_i$. Then, the kernel of the curl operator in $H_0(\mathrm{curl}, \Omega_i)$ is $\nabla H_0(\mathrm{grad}, \Omega_i)$ and that of $H(\mathrm{curl}, \Omega_i)$ is $\nabla H(\mathrm{grad}, \Omega_i)$, etc.; see, e.g., [9]. The subdomain boundaries can be quite irregular; see Assumption 1 and Definition 3.1. We denote by H_i = diameter (Ω_i). The interface of the domain decomposition is given by

$$\Gamma := \left(\bigcup_{i=1}^{N} \partial\Omega_i \right) \backslash \partial\Omega,$$

and the contribution to Γ from $\partial\Omega_i$ by $\Gamma_i := \partial\Omega_i \backslash \partial\Omega$. These sets are unions of subdomain edges and vertices. The subdomain edge $\mathcal{E}^{ij}$ common to Ω_i and Ω_j is typically defined as $\partial\Omega_i \cap \partial\Omega_j$ excluding the two subdomain vertices at its endpoints. We note that the intersection of the two subdomain boundaries might have several components. In such a case, each component will be regarded as an edge; this will not cause any extra complications.

We assume a shape-regular triangulation $\mathcal{T}_{h_i}$ of each Ω_i with nodes matching across the interfaces. The smallest element diameter of $\mathcal{T}_{h_i}$ is denoted by h_i and the smallest angle in the triangulation $\mathcal{T}_{h_i}$ of Ω_i is bounded from below by a mesh independent constant.

Associated with the triangulation $\mathcal{T}_{h_i}$ are the two finite element spaces $W^{h_i}_{\mathrm{grad}} \subset H(\mathrm{grad}, \Omega_i)$ and $W^{h_i}_{\mathrm{curl}} \subset H(\mathrm{curl}, \Omega_i)$ based on continuous, piecewise linear, triangular nodal elements and linear, triangular edge (Nédeléc) elements, respectively. We could equally well develop our algorithm and theory for low order quadrilateral elements.

The energy of a vector function $\boldsymbol{u} \in H(\mathrm{curl}, \Omega_i)$ for subdomain Ω_i is defined as

$$E_i(\boldsymbol{u}) := \alpha_i(\nabla \times \boldsymbol{u}, \nabla \times \boldsymbol{u})_{\Omega_i} + \beta_i(\boldsymbol{u}, \boldsymbol{u})_{\Omega_i}, \tag{2.1}$$

where α_i and β_i are assumed constant in Ω_i. The unit tangent vector for Γ_i, directed in a counterclockwise sense, is denoted by $\boldsymbol{t}_i$ and we define the tangential component of $\boldsymbol{u}$ on $\partial\Omega_i$ as

$$u_t := \boldsymbol{u} \cdot \boldsymbol{t}_i.$$

We will often consider elements in $W^{h_i}_{\text{curl}}$ which are the minimal energy extension for boundary data of this kind.

Let $\boldsymbol{d}_{\mathcal{E}}$ denote a unit vector in the direction from one endpoint of a subdomain edge $\mathcal{E}$ to the other with the same sense of direction as $\boldsymbol{t}_i$. The distance between these two endpoints is denoted by $d_{\mathcal{E}}$. Thus, $d_{\mathcal{E}}\boldsymbol{d}_{\mathcal{E}}$ is the vector from one endpoint to the other.

The set $\mathcal{S}_{\mathcal{E}}$ of all subdomain edges is defined as

$$\mathcal{S}_{\mathcal{E}} = \{\ \mathcal{E}^{ij} : i < j \text{ and } \mathcal{E}^{ij} \neq \emptyset\}.$$

The set $\mathcal{S}_{\mathcal{E}_i}$ is the subset of subdomain edges, which belong to Γ_i. When there is a need to uniquely define the tangential direction, e.g., in the definition of the coarse basis functions $\boldsymbol{c}_{\mathcal{E}}$, we will select the direction given for the relevant subdomain with the smaller index.

The coarse basis function $\boldsymbol{c}_{\mathcal{E}}$ for $\mathcal{E} \in \mathcal{S}_{\mathcal{E}}$ is defined such that its tangential component vanishes on $\Gamma \cup \partial\Omega$ except on $\mathcal{E}$ where $\boldsymbol{c}_{\mathcal{E}} \cdot \boldsymbol{t}_i = \boldsymbol{d}_{\mathcal{E}} \cdot \boldsymbol{t}_i$. We note that if $\mathcal{E}$ is a straight edge, then $\boldsymbol{d}_{\mathcal{E}} = \boldsymbol{t}_i$ so that $\boldsymbol{c}_{\mathcal{E}} \cdot \boldsymbol{t}_i = 1$. The coarse basis function $\boldsymbol{c}_{\mathcal{E}}$ is obtained by the energy minimizing extension of the tangential data $\boldsymbol{c}_{\mathcal{E}} \cdot \boldsymbol{t}_i$ into the interior of the two subdomains sharing $\mathcal{E}$. Thus, the construction of a coarse basis function requires the solution of a Dirichlet problem with inhomogeneous boundary data for each of the two subdomains that share the edge. We note that if all the subdomains are triangular, then the coarse basis functions could be the standard Nédeléc basis functions for the coarse triangulation. However, to succeed in the mass-dominated case, we should instead use functions that provide minimum energy extensions of the values on the interface.

Our coarse interpolant of $\boldsymbol{u}$ for our iterative substructuring algorithm (as well as for an overlapping Schwarz algorithm) can be defined as

$$\boldsymbol{u}_0 := \sum_{\mathcal{E} \in \mathcal{S}_{\mathcal{E}}} \bar{u}_{\mathcal{E}} \boldsymbol{c}_{\mathcal{E}}, \quad \text{where} \quad \bar{u}_{\mathcal{E}} := (1/d_{\mathcal{E}}) \int_{\mathcal{E}} u_t \, ds. \tag{2.2}$$

Let $\boldsymbol{N}^{h_i}_e \in W^{h_i}_{\text{curl}}$ and $\boldsymbol{t}^{h_i}_e$ denote the finite element shape function and unit tangent vector, respectively, for an edge e of the finite element mesh $\mathcal{T}_{h_i}$. We assume that $\boldsymbol{N}^{h_i}_e$ is scaled such that $\boldsymbol{N}^{h_i}_e \cdot \boldsymbol{t}^{h_i}_e = 1$ along e. The *edge* finite element interpolant of a sufficiently smooth vector function $\boldsymbol{u} \in H(\text{curl}, \Omega_i)$ is then defined as

$$\Pi^{h_i}(\boldsymbol{u}) := \sum_{e \in \mathcal{M}^{h_i}} u^{h_i}_e \boldsymbol{N}^{h_i}_e, \quad u^{h_i}_e := (1/|e|) \int_e \boldsymbol{u} \cdot \boldsymbol{t}^{h_i}_e \, ds, \tag{2.3}$$

where $\mathcal{M}^{h_i}$ is the set of edges of $\bar{\Omega}_i$, the closure of Ω_i, and $|e|$ is the length of e.

The *nodal* finite element interpolant of a sufficiently smooth $p \in H(\text{grad}, \Omega_i)$ is defined as

$$I^{h_i}(p) := \sum_{\boldsymbol{v} \in \mathcal{N}^{h_i}} p(\boldsymbol{v}) \phi_v, \tag{2.4}$$

where $\mathcal{N}^{h_i}$ is the set of nodes of $\mathcal{T}_{h_i}$, $p(\boldsymbol{v})$ is the value of p at node $\boldsymbol{v}$, and $\phi_v \in W^{h_i}_{\text{grad}}$ is the shape function for node $\boldsymbol{v}$. A coarse interpolant of p will be introduced in Definition 3.7 and further considered in Lemma 3.8.

3. Technical tools. The auxiliary results presented in this section will be used in the proof of our main result, Theorem 6.1.

Our results apply to subdomains that are *uniform*. According to Jones [13], these domains form the largest family for which a bounded extension of $H(\mathrm{grad},\Omega_i)$ to $H(\mathrm{grad},\mathbb{R}^2)$ is possible; we note that they are also known as $(\epsilon,\delta)-$domains. We also note that a uniform domain needs not have a uniformly Lipschitz continuous boundary. Thus, snowflake domains, as in [5, Figs. 5.1 and 5.3] and [15, Figs. 5.3 and 5.4], with fractal boundaries are in this class.

DEFINITION 3.1. *(Uniform Domain). A bounded domain $\Omega\subset\mathbb{R}^n$ is uniform if there exists a constant $C_U(\Omega)>0$ such that for any pair $\mathbf{x}$, $\mathbf{y}$ of points in the closure of Ω, there is a curve $\gamma(t):[0,\ell]\to\Omega$, parametrized by arc length, such that $\gamma(0)=\mathbf{x}$, $\gamma(\ell)=\mathbf{y}$,*

$$\ell \le C_U(\Omega)|\boldsymbol{x}-\boldsymbol{y}|, \quad \textit{and} \tag{3.1}$$

$$\min(|\gamma(t)-\boldsymbol{x}|,|\gamma(t)-\boldsymbol{y}|) \le C_U(\Omega)\cdot dist(\gamma(t),\partial\Omega). \tag{3.2}$$

REMARK 1. *There are several alternative and equivalent definitions. Thus, the left hand side of (3.2) can be replaced by*

$$\min_t(t,\ell-t) \quad \textit{or by} \quad \frac{|\gamma(t)-\boldsymbol{x}||\gamma(t)-\boldsymbol{y}|}{|\boldsymbol{x}-\boldsymbol{y}|}.$$

REMARK 2. *For a rectangular domain of width L_1 and height L_2, one can show that C_U is no less than L_1/L_2. Thus, the constants in our estimates can be large when one or more of the subdomains has a large aspect ratio.* Any good result on the convergence of a domain decomposition algorithm with two or more levels requires the use of

LEMMA 3.2 (Poincaré's inequality). *Consider a domain $\Omega\subset\mathbf{R}^2$. Then,*

$$\|u-\bar{u}_\Omega\|^2_{L^2(\Omega)} \le (\gamma(\Omega,2))^2|\Omega|\|\nabla u\|^2_{L^2(\Omega)}, \quad \forall u\in H(grad,\Omega).$$

This is [5, Lemma 2.2]. Here $\bar{u}_\Omega$ is the average of the scalar function u over Ω, and $\gamma(\Omega,2)$ a parameter in an isoperimetric inequality as in cf. [5, Lemma 2.1]; see that paper for references to the literature. Since any simply connected uniform domain is a John domain and, according to [3], any John domain in the plane has a finite $\gamma(\Omega,2)$, we can use Poincaré's inequality for any uniform domain.

ASSUMPTION 1. *The subdomains Ω_i are all uniform domains and their uniformity constants $C_U(\Omega_i)$ are uniformly bounded from above by a mesh independent constant C_U.*

DEFINITION 3.3. *Let $\mathbf{a}$ and $\mathbf{b}$ denote the two endpoints of an edge $\mathcal{E}=\mathcal{E}^{ij}\in\mathcal{S}_{\mathcal{E}_i}$. The region $R_\mathcal{E}$ is defined as the open set with boundary*

$$\partial R_\mathcal{E} = \gamma_{ab}\cup\mathcal{E},$$

where γ_{ab} is the curve γ in Definition 3.1 for Ω_i with $\mathbf{x}=\mathbf{a}$ and $\mathbf{y}=\mathbf{b}$.

LEMMA 3.4. *For the region $R_\mathcal{E}$ in Definition 3.3, it holds*

$$|R_\mathcal{E}| \le (C_U^2/\pi)d_\mathcal{E}^2, \tag{3.3}$$

$$diam(R_\mathcal{E}) \le (2C_U-1)d_\mathcal{E} \tag{3.4}$$

where $|R_{\mathcal{E}}|$ is the area of $R_{\mathcal{E}}$ and $d_{\mathcal{E}}$ is the distance between the endpoints $\mathbf{a}$ *and* $\mathbf{b}$ *of the edge $\mathcal{E}$.*

Proof. Let $\widetilde{\gamma}_{ab}$ denote the curve γ of Definition 3.1 for Ω_j, the other subdomain which has the edge $\mathcal{E}$ in common with Ω_i, with $\mathbf{x} = \mathbf{a}$ and $\mathbf{y} = \mathbf{b}$. Since both Ω_i and Ω_j are uniform domains, the arc lengths of γ_{ab} and $\widetilde{\gamma}_{ab}$ are bounded by $C_U d_{\mathcal{E}}$. With reference to Figure 3.1, we now define the region $\widetilde{R}_{\mathcal{E}}$ as the open set with boundary

$$\partial \widetilde{R}_{\mathcal{E}} = \gamma_{ab} \cup \widetilde{\gamma}_{ab},$$

and note that the length of the perimeter of $\widetilde{R}_{\mathcal{E}}$ does not exceed $2C_U d_{\mathcal{E}}$. Since a circle maximizes area for a given perimeter, it follows that $|\widetilde{R}_{\mathcal{E}}| \leq C_U^2 d_{\mathcal{E}}^2/\pi$. The bound in (3.3) then follows directly since $R_{\mathcal{E}} \subset \widetilde{R}_{\mathcal{E}}$. The bound in (3.4) also follows from simple geometrical considerations since $R_{\mathcal{E}}$ can always be circumscribed by a circle of diameter no greater than $(2C_U - 1)d_{\mathcal{E}}$. ∎

LEMMA 3.5. *Given a uniform subdomain Ω_i and a connected subset $\mathcal{E} \subset \partial\Omega_i$, there exists a uniform domain $\widehat{\mathcal{R}}_{\mathcal{E}}$, which is a union of finite elements of Ω_i, such that $\mathcal{R}_{\mathcal{E}} \subset \widehat{\mathcal{R}}_{\mathcal{E}}$, $\partial\widehat{\mathcal{R}}_{\mathcal{E}} \cap \partial\Omega_i = \mathcal{E}$, and*

$$|\widehat{\mathcal{R}}_{\mathcal{E}}| \leq C d_{\mathcal{E}}^2, \tag{3.5}$$

$$diam(\widehat{\mathcal{R}}_{\mathcal{E}}) \leq C d_{\mathcal{E}}. \tag{3.6}$$

Proof. In our construction and proof, we will again use the set $\mathcal{R}_{\mathcal{E}}$ and the curve γ_{ab}; the latter forms the boundary of $\mathcal{R}_{\mathcal{E}}$ together with the subdomain edge $\mathcal{E}$. We extend this domain to

$$\widehat{\mathcal{R}}_{\mathcal{E}} := \mathcal{R}_{\mathcal{E}} \cup \mathcal{C}_{ab},$$

where $\mathcal{C}_{ab}$ is the union of two sets of open circular disks $\{B_k\}_0^\infty$ and $\{B'_k\}_0^\infty$. These disks are all centered on γ_{ab} as in [5, Proof of Lemma 4.4]. At the end of the proof, we will also include all of the elements which intersect $\mathcal{C}_{ab}$ in part into $\widehat{\mathcal{R}}_{\mathcal{E}}$ thereby making it the union of elements as is required; the modifications required of our constructions and proofs are relatively minor.

We note that the uniformity constants of $\widehat{\mathcal{R}}_{\mathcal{E}}$ can exceed that of Ω_i. With a considerable effort, we could estimate the new uniformity constant in terms of that of Ω_i; we will however not undertake that exercise here.

The disk B_k is centered at $\boldsymbol{x}_k \in \gamma_{ab}$ and has a radius $r_k := |\boldsymbol{a} - \boldsymbol{x}_k|/(4C_U)$, for $k \geq 1$. The first of the centers, $\boldsymbol{x}_0$, is located in the middle of the curve γ_{ab}, i.e., it is equidistant to $\boldsymbol{a}$ and $\boldsymbol{b}$. The first circular disk $B_0 = B'_0$ has a radius $r_0 := dist(\boldsymbol{x}_0, \partial\Omega_i)/4$. We define the other $\boldsymbol{x}_k$ recursively as the last point of exit of γ_{ab} from B_{k-1} when moving towards $\boldsymbol{a}$. Indeed, we can establish that $\boldsymbol{x}_k \to \boldsymbol{a}$ as $k \to \infty$. Similarly, we also construct the second set of circular disks $\{B'_k\}$, starting at $\boldsymbol{x}'_0 = \boldsymbol{x}_0$, but with centers $\boldsymbol{x}'_k$ located between $\boldsymbol{x}_0$ and $\boldsymbol{b}$ and where $\boldsymbol{x}'_k \to \boldsymbol{b}$ as $k \to \infty$. We note that bounds on the diameter and area of the domain $\widehat{\mathcal{R}}_{\mathcal{E}}$ now follows easily from Lemma 3.4 and elementary considerations.

We now modify the curve γ_{ab}, as in our previous paper, replacing it by a continuous, piecewise linear curve $\widehat{\gamma}_{ab}$ connecting the consecutive centers $\boldsymbol{x}_k$, and $\boldsymbol{x}'_k$, of the two sets of circular disks. We note that the new curve will be shorter than the one it replaces and is generally more regular.

This curve and these disks are considered in some detail in [5]. There it is established that no point in Ω_i belongs to more than a fixed number, $M(C_U)$, of disks and

that intersecting disks have comparable radii. From this fact, we can establish that the arc length along $\widehat{\gamma}_{ab}$ cannot grow faster than a constant times the distance from the nearest endpoint of the edge $\mathcal{E}$; the arc length will of course also be bounded from below by that distance. We note that consecutive disks overlap creating a neighborhood of the curve $\widehat{\gamma}_{ab}$, which at any point on the curve has a width uniformly bounded from below in terms of the radii of the local circular disks. This follows from the fact that the radii of intersecting disks are comparable and that $\boldsymbol{x}_k$, by construction, lies on the boundary of B_k.

We now consider an arbitrary pair of points $\boldsymbol{c}$ and $\boldsymbol{d}$ in $\widehat{\mathcal{R}}_{\mathcal{E}}$. Given that they both belong to Ω_i and that Ω_i is uniform, there is a curve γ_{cd} in the subdomain which connects them and which satisfies the two conditions of Definition 3.1. We replace this curve by $\widehat{\gamma}_{cd}$ constructed in the same way as $\widehat{\gamma}_{ab}$ and denote by $\mathcal{C}_{cd}$ the union of the circular disks involved in the construction of that curve. If this set is contained in $\widehat{\mathcal{R}}_{\mathcal{E}}$, we can accept the curve $\widehat{\gamma}_{cd}$ for this pair of points.

In our discussion below, we will modify the construction of these circular disks making them smaller by using a constant factor λ larger than 4 in the definition of their radii. The estimate of C_U for $\widehat{\mathcal{R}}_E$ then needs to be increased.

There are several cases to consider. We first assume that both $\boldsymbol{c}$ and $\boldsymbol{d}$ lie between $\mathcal{E}$ and $\widehat{\gamma}_{ab}$. Let $\boldsymbol{y}_\ell$ be one of the centers of the circles of $\mathcal{C}_{cd}$, which is closer to $\boldsymbol{c}$ than to $\boldsymbol{d}$, and let its radius be defined by $r_\ell := |\boldsymbol{c} - \boldsymbol{y}_\ell|/(\lambda C_U)$. Since $\boldsymbol{a} \in \partial\Omega_i$, we have $|\boldsymbol{y}_\ell - \boldsymbol{a}| \geq \lambda r_\ell$; we assume without loss of generality that $\boldsymbol{a}$ is the endpoint of $\mathcal{E}$ closest to $\boldsymbol{y}_\ell$.

We now assume that the circle centered at $\boldsymbol{y}_\ell$ and with radius r_ℓ intersects a circle of $\mathcal{C}_{ab}$ centered at $\boldsymbol{x}_k$ and with radius $r_k = |\boldsymbol{a} - \boldsymbol{x}_k|/(4C_U)$. We then have $|\boldsymbol{y}_\ell - \boldsymbol{x}_k| \leq r_k + r_\ell$ and

$$4C_U r_k = |\boldsymbol{a} - \boldsymbol{x}_k| \geq |\boldsymbol{y}_\ell - \boldsymbol{a}| - |\boldsymbol{y}_\ell - \boldsymbol{x}_k| \geq (\lambda - 1)r_\ell - r_k.$$

By selecting $\lambda(C_U)$ sufficiently large and using the fact that the width of the set $\mathcal{C}_{ab}$ can be bounded locally from below in terms of r_k, we find that we can guarantee that the circle centered at $\boldsymbol{y}_\ell$ is contained in $\widehat{\mathcal{R}}_{\mathcal{E}}$ if $\boldsymbol{y}_\ell$ lies between $\mathcal{E}$ and $\widehat{\gamma}_{ab}$. We can therefore change our focus to cases when the two curves $\widehat{\gamma}_{ab}$ and $\widehat{\gamma}_{cd}$ intersect since we have shown that otherwise both requirements of Definition 3.1 can be satisfied.

If $\widehat{\gamma}_{cd}$ intersects $\widehat{\gamma}_{ab}$, it must do so at least twice given that $\boldsymbol{c}$ and $\boldsymbol{d}$, by assumption, lie on the same side of $\widehat{\gamma}_{ab}$. Denote the first and last such intersection by $\boldsymbol{x}_c$ and $\boldsymbol{x}_d$, respectively. We then replace the part of $\widehat{\gamma}_{cd}$ between $\boldsymbol{x}_c$ and $\boldsymbol{x}_d$ by that of $\widehat{\gamma}_{ab}$ creating a modified curve still denoted by $\widehat{\gamma}_{cd}$.

We need to verify that the two conditions of Definition 3.1 can be satisfied after possibly increasing the parameter C_U.

We first consider the length. The length of the parts of the original $\widehat{\gamma}_{cd}$ that are retained can clearly be estimated by $C_U|\boldsymbol{c} - \boldsymbol{d}|$. We can estimate $|\boldsymbol{x}_c - \boldsymbol{x}_d|$ similarly. As indicated above, the arc length of the part of $\widehat{\gamma}_{ab}$ which is incorporated into $\widehat{\gamma}_{cd}$ can then also be estimated by a multiple of $|\boldsymbol{x}_c - \boldsymbol{x}_d|$. We note that we again might have to increase the value of C_U.

We next show that the circular disks of $\mathcal{C}_{ab}$ centered on $\widehat{\gamma}_{ab}$ are large enough to accommodate the circular disks centered on $\widehat{\gamma}_{cd}$ after a possible increase of the C_U parameter necessary for $\widehat{\gamma}_{cd}$. This can fail only if $|\boldsymbol{c} - \boldsymbol{x}|$, with $\boldsymbol{x} \in \widehat{\gamma}_{cd}$, cannot be bounded in terms of $|\boldsymbol{a} - \boldsymbol{x}|$. This cannot happen since the arc length between $\boldsymbol{a}$ and $\boldsymbol{x}_c$ can be bounded from below by the radii of the circles centered close to $\boldsymbol{x}_c$. That radius in turn provides a bound on the arc length between $\boldsymbol{c}$ and $\boldsymbol{x}_c$. We note

that along the common part of $\widehat{\gamma}_{cd}$ and $\widehat{\gamma}_{ab}$ the arc lengths of $\widehat{\gamma}_{ab}$ and $\widehat{\gamma}_{cd}$ increase at exactly the same rate. This ultimately provides a bound on $|\boldsymbol{c}-\boldsymbol{x}|$ in terms of $|\boldsymbol{a}-\boldsymbol{x}|$ for any point $\boldsymbol{x}$ on the common part of the two curves; this will guarantee that $\mathcal{C}_{ab}$ is wide enough.

To make the argument complete, we must also consider possible points on the common part of the curve beyond $\boldsymbol{x}_0$, where the width of $\mathcal{C}_{ab}$ can begin to shrink. We can then work from the other end point of $\widehat{\gamma}_{cd}$, i.e., start from $\boldsymbol{d}$.

There are also other cases to consider. Thus, if both $\boldsymbol{c}$ and $\boldsymbol{d}$ both belong to $\mathcal{C}_{ab}$, we can use the fact that this set is uniform in itself. There are two cases. In the first case, we can construct $\widehat{\gamma}_{cd}$ by connecting $\boldsymbol{c}$ and $\boldsymbol{d}$ by straight line segments to the points on $\widehat{\gamma}_{ab}$ that are closest and the part of that curve in between. We note that the distances of those two points to that curve provide lower bounds on the radii of the circles of $\mathcal{C}_{ab}$ to which they belong. However, this can lead to a curve that is too long in comparison with $|\boldsymbol{c}-\boldsymbol{d}|$ if the distance of $\boldsymbol{c}$ or $\boldsymbol{d}$ to $\widehat{\gamma}_{ab}$ far exceeds $|\boldsymbol{c}-\boldsymbol{d}|$. But in such a case $\boldsymbol{c}$ and $\boldsymbol{d}$ must belong to the same circular disk or to two consecutive disks in the sets of circles and it is then easy to construct a satisfactory curve $\widehat{\gamma}_{cd}$ taking advantage of the simple geometry.

Finally, let $\boldsymbol{c}$ and $\boldsymbol{d}$ lie on opposite sides of $\widehat{\gamma}_{ab}$ and let $\boldsymbol{c} \in \mathcal{R}_{\mathcal{E}} \setminus \mathcal{C}_{ab}$. We then find the first intersection of $\widehat{\gamma}_{cd}$ and $\widehat{\gamma}_{ab}$ when moving from $\boldsymbol{c}$ along $\widehat{\gamma}_{cd}$. We connect $\boldsymbol{d}$ by a straight line segment to the point on $\widehat{\gamma}_{ab}$ that is closest and then build the modified curve from the resulting three parts. We note that in this case, we will not have a problem with $\boldsymbol{c}$ and $\boldsymbol{d}$ being too close.

To complete the proof, we add all the parts of any elements that intersect $\widehat{\mathcal{R}}_{\mathcal{E}}$ to the set; effectively this will increase the set $\mathcal{C}_{ab}$. Should $\boldsymbol{c}$ or $\boldsymbol{d}$ or both belong to this new part, we can connect these points to points just inside $\mathcal{C}_{ab}$ and construct $\widehat{\gamma}_{cd}$ by using the same ideas as previously. ∎

We note that estimates closely related to those of the next lemma are presented in [5] and, in particular, in [15, Lemma 4.4] for the more general class of John domains. The motivation for considering uniform domains rather than John domains stems from the need to have a factor of $d_{\mathcal{E}}^2$ rather than H_i^2 in (3.8) in an estimate of the L^2-norm of certain edge functions. This is motivated by the need to prove the existence of low energy coarse interpolants for mass-dominated cases. The new proof is quite different and, we believe, of independent interest. We will now rely on the fact that the curve γ_{ab} satisfies the conditions of Definition 3.1.

LEMMA 3.6. *Let $\mathcal{E} \in \mathcal{S}_{\mathcal{E}_i}$ with endpoints* **a** *and* **b**. *There exists an edge function $\vartheta_{\mathcal{E}} \in W^{h_i}_{grad}$ equal to 1 at all nodes of $\mathcal{E}$ and vanishing at all other nodes on $\partial\Omega_i$ such that*

$$(\nabla\vartheta_{\mathcal{E}}, \nabla\vartheta_{\mathcal{E}})_{\Omega_i} \leq C(1+\log(d_{\mathcal{E}}/h_i)), \tag{3.7}$$

$$(\vartheta_{\mathcal{E}}, \vartheta_{\mathcal{E}})_{\Omega_i} \leq C d_{\mathcal{E}}^2. \tag{3.8}$$

Proof. We first rename the edge $\mathcal{E} =: \mathcal{E}_1$ and introduce the additional notation $\mathcal{E}_2 := \partial R_{\mathcal{E}} \setminus \mathcal{E}$. We next define, for $x \in R_{\mathcal{E}}$,

$$\widetilde{\vartheta}_{\mathcal{E}}(\mathbf{x}) := \frac{1/d_1(\mathbf{x})}{1/d_1(\mathbf{x}) + 1/d_2(\mathbf{x})}, \tag{3.9}$$

where $d_i(\mathbf{x})$ is the distance of $\mathbf{x}$ to the edge $\mathcal{E}_i, i = 1, 2$. We then extend $\widetilde{\vartheta}_{\mathcal{E}}$ by 0 for $x \in \Omega_i \setminus R_{\mathcal{E}}$.

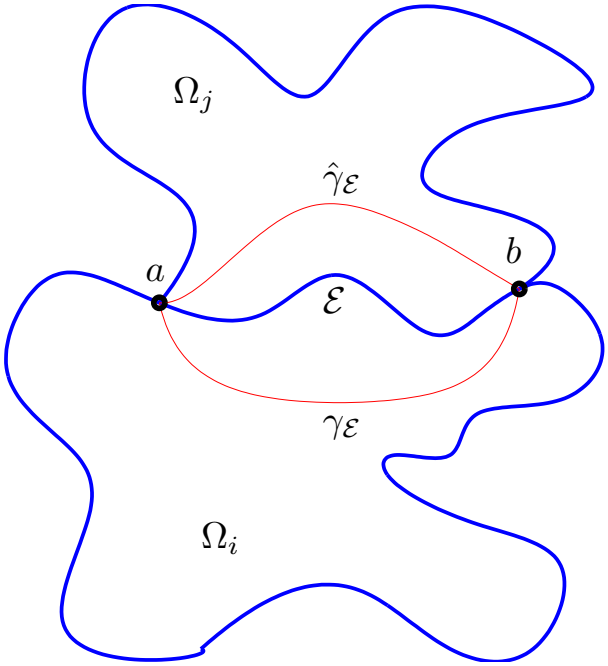

FIG. 3.1. *Figure showing geometry of an edge* $\mathcal{E} = \mathcal{E}^{ij}$. *The distance between the edge endpoints* $\mathbf{a}$ *and* $\mathbf{b}$ *is denoted by* $d_{\mathcal{E}}$.

This formula provides the correct boundary values at all interior nodes of $\mathcal{E}_1$ and at all interior points of $\mathcal{E}_2$. At the endpoints of the edges, i.e., at $\mathbf{a}$ and $\mathbf{b}$, where $\widetilde{\vartheta}_{\mathcal{E}}$ is not well defined by (3.9); we set the value of this function to 0 at those two points. We note that the contribution of any element, with $\mathbf{a}$ or $\mathbf{b}$ as a vertex, to the energy of the finite element interpolant $\vartheta_{\mathcal{E}} := I_i^h(\widetilde{\vartheta}_{\mathcal{E}})$ will be bounded since all its nodal values are between 0 and 1. Its gradient can therefore be bounded by the inverse of the local mesh size.

We note that in our final estimate, we can use an estimate of the maximum of $|\nabla\widetilde{\vartheta}_{\mathcal{E}}|$ over individual elements since the same estimate also holds for its piecewise linear interpolant $\vartheta_{\mathcal{E}}$.

We now focus on the contributions of all the elements of the domain, which are not next to the two subdomain vertices, and thus are at a distance exceeding $ch_i, c > 0$, from $\boldsymbol{a}$ and $\boldsymbol{b}$. We denote this domain by Ω_i'.

We easily find that

$$\nabla\widetilde{\vartheta}_{\mathcal{E}}(\mathbf{x}) = \frac{-d_2\nabla d_1 + d_1\nabla d_2}{(d_1+d_2)^2}.$$

Since $|\nabla d_i| \leq 1$, we obtain

$$|\nabla\widetilde{\vartheta}_{\mathcal{E}}(\mathbf{x})| \leq \frac{1}{d_1(\mathbf{x})+d_2(\mathbf{x})}.$$

Since the domain is uniform, we can bound $d_1(\mathbf{x}) + d_2(\mathbf{x})$ from below by $cr(\mathbf{x})$ where $r(\mathbf{x})$ is the minimal distance of $\mathbf{x}$ to $\mathbf{a}$ and $\mathbf{b}$ and $c > 0$ a constant. We can prove this by considering $\mathbf{x}_1 \in \mathcal{E}_1$ and $\mathbf{x}_2 \in \mathcal{E}_2$, points that are closest to $\mathbf{x} \in R_{\mathcal{E}}$ in the respective

sets. Let us assume, without a loss in generality, that $\boldsymbol{x}_2$ is closer to $\boldsymbol{a}$ than to $\boldsymbol{b}$. We also have $|\mathbf{x}_1 - \mathbf{x}| = d_1(\mathbf{x})$ and $|\mathbf{x}_2 - \mathbf{x}| = d_2(\mathbf{x})$ and, by the triangle inequality, $|\mathbf{x}_1 - \mathbf{x}_2| \leq d_1(\mathbf{x}) + d_2(\mathbf{x})$. Therefore, $dist(\mathbf{x}_2, \mathcal{E}_1) \leq |\mathbf{x}_1 - \mathbf{x}_2| \leq d_1(\mathbf{x}) + d_2(\mathbf{x})$. We can now obtain a lower bound of $dist(\mathbf{x}_2, \mathcal{E}_1)$ in terms of $|\mathbf{x}_2 - \mathbf{a}|$ by using (3.2). By using the triangle inequality, we find that $C_U dist(\mathbf{x}_2, \mathcal{E}_1) \geq |\mathbf{x} - \mathbf{a}| - d_2(\mathbf{x})$ and therefore

$$r(\mathbf{x}) := |\mathbf{x} - \mathbf{a}| \leq C_U(d_1(\mathbf{x}) + d_2(\mathbf{x})) + d_2(\mathbf{x}) \leq (C_U + 1)(d_1(\mathbf{x}) + d_2(\mathbf{x})).$$

The same type of bounds can also be derived for points $\boldsymbol{x}_2$ closer to $\boldsymbol{b}$ than to $\boldsymbol{a}$; then $r(\mathbf{x}) := |\mathbf{x} - \mathbf{b}|$, etc. Thus, we find,

$$\int_{\Omega_i} |\nabla \widetilde{\vartheta}_{\mathcal{E}}|^2 \leq C + (C_U + 1)^2 \int_{\Omega_i'} \frac{dx}{r(\mathbf{x})^2}.$$

The bound (3.7) then follows easily by using polar coordinates centered at $\boldsymbol{a}$ and $\boldsymbol{b}$.

Finally, the bound (3.8) follows easily from Lemma 3.4 and the fact that $0 \leq \vartheta_{\mathcal{E}} \leq 1$ and that this function vanishes in all elements that are entirely outside of $R_{\mathcal{E}}$. □

We note that we can obtain the same result for the domain $\widehat{\mathcal{R}}_{\mathcal{E}}$ as for $\mathcal{R}_{\mathcal{E}}$, since $\mathcal{R}_{\mathcal{E}} \subset \widehat{\mathcal{R}}_{\mathcal{E}}$, by simply extending $\vartheta_{\mathcal{E}}$ by zero in $\widehat{\mathcal{R}}_{\mathcal{E}} \setminus \mathcal{R}_{\mathcal{E}}$.

We next introduce a coarse linear interpolant f_ℓ of an arbitrary element $f \in W^{h_i}_{\text{grad}}$; we note that while f_ℓ will not belong to $W^{h_i}_{\text{curl}}$, its gradient will and its tangential derivative on the interface will therefore equal the trace of an element in $W^{h_i}_{\text{curl}}$. In fact, this trace will equal that of an element of our coarse space introduced in Section 2. We note that this linear interpolant is only a theoretical tool and is never calculated.

DEFINITION 3.7. *(Linear Interpolant). Given $f \in W^{h_i}_{grad}$ and a subdomain edge $\mathcal{E} \in \mathcal{S}_{\mathcal{E}_i}$, we define the linear function*

$$f^{\mathcal{E}\ell} := f(\boldsymbol{a}) + \frac{f(\boldsymbol{b}) - f(\boldsymbol{a})}{d_{\mathcal{E}}}(\boldsymbol{x} - \boldsymbol{a}) \cdot \boldsymbol{d}_{\mathcal{E}}. \tag{3.10}$$

We note that $f^{\mathcal{E}\ell}$ equals f at the two endpoints of $\mathcal{E}$ and varies linearly in the direction $\boldsymbol{d}_{\mathcal{E}}$.

LEMMA 3.8. *Let $\widehat{\mathcal{R}}_{\mathcal{E}}$ be the uniform domain of Lemma 3.5. For any $f \in W^{h_i}_{grad}$, there exists a function $f^{\mathcal{E}\Delta} \in W^{h_i}_{grad}$ such that $f^{\mathcal{E}\Delta} = f - f^{\mathcal{E}\ell}$ along $\mathcal{E}$. This function vanishes along both $\partial\widehat{\mathcal{R}}_{\mathcal{E}} \setminus \mathcal{E}$ and $\partial\Omega_i \setminus \mathcal{E}$, and satisfies*

$$|f^{\mathcal{E}\Delta}|^2_{H(grad,\Omega_i)} \leq C(1 + \log(d_{\mathcal{E}}/h_i))^2 |f|^2_{H(grad,\widehat{\mathcal{R}}_{\mathcal{E}})}. \tag{3.11}$$

Proof. We first note that since by Lemma 3.5 $|\boldsymbol{x} - \boldsymbol{a}| \leq C d_{\mathcal{E}}$, $\forall \boldsymbol{x} \in \widehat{\mathcal{R}}_{\mathcal{E}}$,

$$\|f^{\mathcal{E}\ell} - f(\boldsymbol{a})\|_{L^\infty(\widehat{\mathcal{R}}_{\mathcal{E}})} \leq C|f(\boldsymbol{b}) - f(\boldsymbol{a})|. \tag{3.12}$$

To estimate the maximum difference of f at any two points in $\widehat{\mathcal{R}}_{\mathcal{E}}$, we use a well-known finite element Sobolev inequality

$$\|f_{\max} - f_{\min}\|^2_{L^\infty(\widehat{\mathcal{R}}_{\mathcal{E}})} \leq C(1 + \log(d_{\mathcal{E}}/h_i))|f|^2_{H(\text{grad},\widehat{\mathcal{R}}_{\mathcal{E}})}, \tag{3.13}$$

which has been established for John domains in [5, Lemma 3.2], and thus also holds for uniform domains. Since $f - f^{\mathcal{E}\ell} = (f - f(\boldsymbol{a})) - (f^{\mathcal{E}\ell} - f(\boldsymbol{a}))$, we have

$$\|f - f^{\mathcal{E}\ell}\|^2_{L^\infty(\widehat{\mathcal{R}}_{\mathcal{E}})} \leq C(1 + \log(d_{\mathcal{E}}/h_i))|f|^2_{H(\text{grad},\widehat{\mathcal{R}}_{\mathcal{E}})},$$
$$|f^{\mathcal{E}\ell}|_{H(\text{grad},\widehat{\mathcal{R}}_{\mathcal{E}})} \leq C(1 + \log(d_{\mathcal{E}}/h_i))^2 |f|^2_{H(\text{grad},\widehat{\mathcal{R}}_{\mathcal{E}})}.$$

From the previous two estimates, Lemma 3.6, and

$$\nabla(\vartheta_{\mathcal{E}}(f - f^{\mathcal{E}\ell})) = \nabla\vartheta_{\mathcal{E}}(f - f^{\mathcal{E}\ell}) + \nabla(f - f^{\mathcal{E}\ell})\vartheta_{\mathcal{E}},$$

we find that

$$|\vartheta_{\mathcal{E}}(f - f^{\mathcal{E}\ell})|^2_{H(\mathrm{grad},\Omega_i)} \leq C(1 + \log(d_{\mathcal{E}}/h_i)^2|f|^2_{H(\mathrm{grad},\widehat{\mathcal{R}}_{\mathcal{E}})}$$

since $|\vartheta_{\mathcal{E}}| \leq 1$ and $\vartheta_{\mathcal{E}}$ vanishes in $\Omega_i \setminus \widehat{\mathcal{R}}_{\mathcal{E}}$. The lemma now follows from the definition $f^{\mathcal{E}\Delta} := I^{h_i}(\vartheta_{\mathcal{E}}(f - f^{\mathcal{E}\ell}))$ and [24, Lemma 4.31]; that lemma shows that we can bound the norm of the piecewise linear interpolant of the product of two piecewise linear functions by the norm of their product. ∎

Later in the analysis, we will need a bound on the average tangential component of the gradient of a function $f \in W^{h_i}_{\mathrm{grad}}$ along an edge $\mathcal{E} \in \mathcal{S}_{\mathcal{E}_i}$. Consider an element with an edge $e \subset \mathcal{E} \subset \partial\Omega_i$. For linear finite elements, $\nabla f \cdot \boldsymbol{t}_i$ is constant on e, and the difference in nodal values along this edge is $|e|\nabla f \cdot \boldsymbol{t}_i$, where $|e|$ is the length of the edge. Summing these differences over all elements along $\mathcal{E}$, we find that

$$\frac{1}{d_{\mathcal{E}}}\int_{\mathcal{E}} \nabla f \cdot \boldsymbol{t}_i \, ds = \frac{f(\mathbf{b}) - f(\mathbf{a})}{d_{\mathcal{E}}}.$$

The inequalities of the following lemma are two-dimensional counterparts of 3D estimates appearing in Corollary 1 and the proof of Theorem 2 in [16]. They can be derived by arguments for individual elements.

LEMMA 3.9. *Let $K \in \mathcal{T}_{h_i}$. For $\boldsymbol{u} \in (W^{h_i}_{grad})^2$, it holds that*

$$\nabla \times \Pi^{h_i}(\boldsymbol{u}) = \nabla \times \boldsymbol{u}, \tag{3.14}$$

$$\|\Pi^{h_i}(\boldsymbol{u})\|^2_{L^2(K)} \leq C\|\boldsymbol{u}\|^2_{L^2(K)}. \tag{3.15}$$

The next three lemmas and their proofs also hold for connected subsets $\mathcal{E}_k \subset \mathcal{E}$.

LEMMA 3.10. *Given $\boldsymbol{u} \in W^{h_i}_{curl}$ and a subdomain edge $\mathcal{E} \in \mathcal{S}_{\mathcal{E}_i}$, it holds that*

$$|\bar{u}_{\mathcal{E}}|^2 \leq C(\|\boldsymbol{u}\|^2_{L^\infty(\mathcal{R}_{\mathcal{E}})} + \|\nabla \times \boldsymbol{u}\|^2_{L^2(\mathcal{R}_{\mathcal{E}})}).$$

*Here, $\bar{u}_{\mathcal{E}}$ is defined as in (*2.2).

Proof. We first note that the direct use of the Cauchy–Schwarz inequality to estimate $\bar{u}_{\mathcal{E}}$ leads to a difficulty since the length of the edge $\mathcal{E}$ cannot be bounded uniformly in terms of $d_{\mathcal{E}}$, the distance between the endpoints of the edge. However, we have a uniform bound for the length of the curve γ_{ab} of Definition 3.1, which completes the boundary of the domain $\mathcal{R}_{\mathcal{E}}$. By using the Stokes theorem, we find that

$$\int_{\mathcal{E}} \boldsymbol{u} \cdot \boldsymbol{t}_i \, ds = \int_{\mathcal{R}_{\mathcal{E}}} \nabla \times \boldsymbol{u} \, dx - \int_{\partial\mathcal{R}_{\mathcal{E}} \setminus \mathcal{E}} \boldsymbol{u} \cdot \boldsymbol{t}_i \, ds.$$

By Lemma 3.5, the area of $\mathcal{R}_{\mathcal{E}}$ is of order $d^2_{\mathcal{E}}$ and the length of $\gamma_{ab} = \partial\mathcal{R}_{\mathcal{E}} \setminus \mathcal{E}$ is of order $d_{\mathcal{E}}$. The lemma then follows by using the Cauchy-Schwarz inequality and an elementary argument. ∎

We next consider *coarse space* functions. Such a function coincides with an element in our coarse space on the interface, but it is not necessarily of minimal energy.

LEMMA 3.11. *Given $\mathcal{E} \in \mathcal{S}_{\mathcal{E}_i}$, there exists a coarse space function $\boldsymbol{N}_{\mathcal{E}} \in W^{h_i}_{curl}$ with $\boldsymbol{N}_{\mathcal{E}} \cdot \boldsymbol{t}_i = \boldsymbol{d}_{\mathcal{E}} \cdot \boldsymbol{t}_i$ along $\mathcal{E}$ and $\boldsymbol{N}_{\mathcal{E}} \cdot \boldsymbol{t}_i = 0$ elsewhere on $\partial\Omega_i$ such that*

$$\|\boldsymbol{N}_{\mathcal{E}}\|^2_{L^2(\Omega_i)} \leq C d^2_{\mathcal{E}}, \tag{3.16}$$

$$\|\nabla \times \boldsymbol{N}_{\mathcal{E}}\|^2_{L^2(\Omega_i)} \leq C(1 + \log(d_{\mathcal{E}}/h_i)), \tag{3.17}$$

where $d_{\mathcal{E}}$ is the distance between the endpoints of $\mathcal{E}$. Further, $\boldsymbol{N}_{\mathcal{E}}(\boldsymbol{x}) = 0,\ \boldsymbol{x} \in \Omega_i \backslash \widehat{\mathcal{R}}_{\mathcal{E}}$, where $\widehat{\mathcal{R}}_{\mathcal{E}}$ is the domain of Lemma 3.5.

Proof. Let e_a and e_b denote the two finite element edges at the ends of $\mathcal{E}$ and define

$$\boldsymbol{N}_{\mathcal{E}} := \Pi^{h_i}(\vartheta_{\mathcal{E}} \boldsymbol{d}_{\mathcal{E}}) + \boldsymbol{b}_{\mathcal{E}}/2,$$

where $\vartheta_{\mathcal{E}}$ is the edge cutoff function of Lemma 3.6 and

$$\boldsymbol{b}_{\mathcal{E}} := (\boldsymbol{d}_{\mathcal{E}} \cdot \boldsymbol{t}^{h_i}_{e_a}) \boldsymbol{N}_{e_a} + (\boldsymbol{d}_{\mathcal{E}} \cdot \boldsymbol{t}^{h_i}_{e_b}) \boldsymbol{N}_{e_b}.$$

Since $\vartheta_{\mathcal{E}} = 1$ along all edges of $\mathcal{E}$ except for e_a and e_b, we see from (2.3) that $\Pi^{h_i}(\vartheta_{\mathcal{E}} \boldsymbol{d}_{\mathcal{E}}) \cdot \boldsymbol{t}_i = \boldsymbol{d}_{\mathcal{E}} \cdot \boldsymbol{t}_i$ along these interior edges. We also have $\Pi^{h_i}(\vartheta_{\mathcal{E}} \boldsymbol{d}_{\mathcal{E}}) \cdot \boldsymbol{t}_i = \boldsymbol{d}_{\mathcal{E}} \cdot \boldsymbol{t}_i/2$ along e_a and e_b since $\vartheta_{\mathcal{E}}$ varies linearly from 1 to 0 along these two edges. For these two edges, we also have $\boldsymbol{b}_{\mathcal{E}} \cdot \boldsymbol{t}_i = \boldsymbol{d}_{\mathcal{E}} \cdot \boldsymbol{t}_i$ so that $\boldsymbol{N}_{\mathcal{E}}$ has the correct, specified tangential data along $\mathcal{E}$. In addition, the tangential data of $\boldsymbol{N}_{\mathcal{E}}$ also vanishes along $\partial\Omega_i \setminus \mathcal{E}$.

Since $\vartheta_{\mathcal{E}} \boldsymbol{d}_{\mathcal{E}} \in (W^{h_i}_{\text{grad}})^2$ and $\boldsymbol{d}_{\mathcal{E}}$ is a unit vector, it follows from Lemma 3.6 and (3.15) that

$$\|\Pi^{h_i}(\vartheta_{\mathcal{E}} \boldsymbol{d}_{\mathcal{E}})\|^2_{L^2(\Omega_i)} \leq C d^2_{\mathcal{E}}.$$

Again, since $\boldsymbol{d}_{\mathcal{E}}$ is a unit vector, we have that $\|\nabla \times \vartheta_{\mathcal{E}} \boldsymbol{d}_{\mathcal{E}}\|_{L^2(\Omega_i)} \leq \|\nabla \vartheta_{\mathcal{E}}\|_{L^2(\Omega_i)}$. It then follows from Lemma 3.6 and (3.14), that

$$\|\nabla \times \Pi^{h_i}(\vartheta_{\mathcal{E}} \boldsymbol{d}_{\mathcal{E}})\|^2_{L^2(\Omega_i)} \leq C(1 + \log(d_{\mathcal{E}}/h_i)).$$

The coefficients of $\boldsymbol{N}^{h_i}_{e_a}$ and $\boldsymbol{N}^{h_i}_{e_b}$ in the definition of $\boldsymbol{b}_{\mathcal{E}}$ have absolute values bounded by 1. It then follows from elementary finite element estimates that $\|\boldsymbol{b}_{\mathcal{E}}\|^2_{L^2(\Omega_i)} \leq C h_i^2$ and $\|\nabla \times \boldsymbol{b}_{\mathcal{E}}\|^2_{L^2(\Omega_i)} \leq C$. The lemma now follows directly from the estimates for $\Pi^{h_i}(\vartheta_{\mathcal{E}} \boldsymbol{d}_{\mathcal{E}})$ and $\boldsymbol{b}_{\mathcal{E}}$. ∎

The next lemma is a counterpart of Lemma 3.8 for functions in $W^{h_i}_{\text{curl}}$.

LEMMA 3.12. *Given $\boldsymbol{v} \in W^{h_i}_{curl}$ and $\mathcal{E} \in \mathcal{S}_{\mathcal{E}_i}$, there exists a function $\boldsymbol{v}^{\mathcal{E}} \in W^{h_i}_{curl}$ such that $\boldsymbol{v}^{\mathcal{E}} \cdot \boldsymbol{t}_i = \boldsymbol{v} \cdot \boldsymbol{t}_i$ along $\mathcal{E}$ with vanishing tangential data $\boldsymbol{v}^{\mathcal{E}} \cdot \boldsymbol{t}_i$ along both $\partial\widehat{\mathcal{R}}_{\mathcal{E}} \setminus \mathcal{E}$ and $\partial\Omega_i \setminus \mathcal{E}$. Further,*

$$\|\boldsymbol{v}^{\mathcal{E}}\|^2_{L^2(\Omega_i)} \leq C d^2_{\mathcal{E}} \|\boldsymbol{v}\|^2_{L^\infty(\widehat{\mathcal{R}}_{\mathcal{E}})}, \tag{3.18}$$

$$\|\nabla \times \boldsymbol{v}^{\mathcal{E}}\|^2_{L^2(\Omega_i)} \leq C(\|\nabla \times \boldsymbol{v}\|^2_{L^2(\widehat{\mathcal{R}}_{\mathcal{E}})} + (1 + \log(d_{\mathcal{E}}/h_i)) \|\boldsymbol{v}\|^2_{L^\infty(\widehat{\mathcal{R}}_{\mathcal{E}})}). \tag{3.19}$$

Proof. Referring to (2.3), we have

$$\boldsymbol{v} = \sum_{e \in \mathcal{M}^{h_i}} v_e \boldsymbol{N}_e.$$

As in Lemma 3.11, let e_a and e_b denote the edges at the ends of $\mathcal{E}$. Similar to what was done in the proof of that lemma, we define

$$\boldsymbol{v}^{\mathcal{E}} := \sum_{e\in\mathcal{M}^{h_i}} \vartheta^e_{\mathcal{E}} v_e \boldsymbol{N}_e + (v_{e_a}\boldsymbol{N}_{e_a} + v_{e_b}\boldsymbol{N}_{e_b})/2,$$

where $\vartheta^e_{\mathcal{E}}$ is the value of $\vartheta_{\mathcal{E}}$ at the center of edge e. We can confirm that $\boldsymbol{v}^{\mathcal{E}}\cdot\boldsymbol{t}_i = \boldsymbol{v}\cdot\boldsymbol{t}_i$ along $\mathcal{E}$ and that $\boldsymbol{v}^{\mathcal{E}}\cdot\boldsymbol{t}_i$ vanishes along $\partial\widehat{\mathcal{R}}_{\mathcal{E}}\setminus\mathcal{E}$ and $\partial\Omega_i\setminus\mathcal{E}$. Since $|\vartheta_{\mathcal{E}}|\le 1$, we find by using the product rule of differentiation and elementary estimates that for element K

$$\begin{aligned}
\|\sum_{e\in\mathcal{S}_K} \vartheta^e_{\mathcal{E}} v_e \boldsymbol{N}_e\|^2_{L^2(K)} &\le C\|\boldsymbol{v}\|^2_{L^2(K)},\\
\|\sum_{e\in\mathcal{S}_K} \nabla\times\vartheta^e_{\mathcal{E}} v_e \boldsymbol{N}_e\|^2_{L^2(K)} &\le C(\|\nabla\times\boldsymbol{v}\|^2_{L^2(K)} + \|\boldsymbol{v}\|^2_{L^\infty(\widehat{\mathcal{R}}_{\mathcal{E}})}\|\nabla\vartheta_{\mathcal{E}}\|^2_{L^2(K)}).
\end{aligned}$$

Estimates for the remaining two terms are easily obtained and are given by

$$\begin{aligned}
\|v_{e_a}\boldsymbol{N}_{e_a} + v_{e_b}\boldsymbol{N}_{e_b}\|^2_{L^2(\Omega_i)} &\le Ch_i^2\|\boldsymbol{v}\|^2_{L^\infty(\widehat{\mathcal{R}}_{\mathcal{E}})},\\
\|\nabla\times(v_{e_a}\boldsymbol{N}_{e_a} + v_{e_a}\boldsymbol{N}_{e_b})\|^2_{L^2(\Omega_i)} &\le C\|\boldsymbol{v}\|^2_{L^\infty(\widehat{\mathcal{R}}_{\mathcal{E}})}.
\end{aligned}$$

The proof is completed by assembling the estimates for the terms that define $\boldsymbol{v}^{\mathcal{E}}$ and by using (3.7). □

In preparation for Lemma 3.13, we consider the number $\chi_{\mathcal{E}}(d)(d_{\mathcal{E}}/d)$ of closed circular disks, of diameter d, that are required to cover a subdomain edge $\mathcal{E}$; we note that $\chi_{\mathcal{E}}(d)$ equals 1 if the edge is straight. This is closely related to the Hausdorff dimension of the edge; see, e.g., [8]. We note that $\chi_{\mathcal{E}}(d)$ increases monotonically when d decreases. By examining the standard computation of the Hausdorff dimension of a Koch snowflake curve, we can, e.g., show that a pre-fractal Koch snowflake curve, which is a polygon with side length h_i and diameter H_i, will satisfy $\chi_{\mathcal{E}}(d)\le (4/3)^{\log(H_i/h_i)}$. This is not a very large factor being less than $4\log(H_i/h_i)$ even in the very extreme case of $H_i/h_i = 10^6$.

REMARK 3. *We note that a factor of $\chi_{\mathcal{E}}(\delta_j)$ was left out of an argument on page 2161 of [5] and in the bound for the condition number given in Theorem 3.1 of that paper. This main result is therefore incorrect. However, we can expect that additional factor to be quite modest in realistic cases.*

LEMMA 3.13. *Given $\mathcal{E}\in\mathcal{S}_{\mathcal{E}_i}$ and $h_i\le d<d_{\mathcal{E}}$, there exists a coarse space function $\boldsymbol{N}_{\mathcal{E}d}\in W^{h_i}_{curl}$ with $\boldsymbol{N}_{\mathcal{E}d}\cdot\boldsymbol{t}_i = \boldsymbol{d}_{\mathcal{E}}\cdot\boldsymbol{t}_i$ along $\mathcal{E}$ and $\boldsymbol{N}_{\mathcal{E}d}\cdot\boldsymbol{t}_i = 0$ elsewhere on $\partial\Omega_i$ such that*

$$\|\boldsymbol{N}_{\mathcal{E}d}\|^2_{L^2(\Omega_i)} \le C\chi_{\mathcal{E}}(d)d_{\mathcal{E}}d, \tag{3.20}$$

$$\|\nabla\times\boldsymbol{N}_{\mathcal{E}d}\|^2_{L^2(\Omega_i)} \le C\chi_{\mathcal{E}}(d)(d_{\mathcal{E}}/d)(1+\log(d/h_i)). \tag{3.21}$$

Proof. Let $\boldsymbol{a}$ and $\boldsymbol{b}$ denote the two endpoints of $\mathcal{E}$. Starting at $\boldsymbol{a}$ and moving along this curve towards $\boldsymbol{b}$, we pick $\boldsymbol{p}_1 := \boldsymbol{a}$ and then $\boldsymbol{p}_2\in\mathcal{E}$ as a node nearest the last point of exit of $\mathcal{E}$ from the circular disk $B(\boldsymbol{p}_1,d)$ of radius d centered at $\boldsymbol{p}_1$. Likewise, $\boldsymbol{p}_3\in\mathcal{E}$ is chosen as a node nearest the last point of exit of $\mathcal{E}$ from $B(\boldsymbol{p}_2,d)$. This process is repeated until $|\boldsymbol{p}_M - \boldsymbol{b}|$ is no larger than $2d$, and we then set $\boldsymbol{p}_{M+1} = \boldsymbol{b}$. We denote the segment of $\mathcal{E}$ between $\boldsymbol{p}_k$ and $\boldsymbol{p}_{k+1}$ by $\mathcal{E}_k$.

From Lemma 3.5, we know that there exists a uniform domain $\widehat{\mathcal{R}}_{\mathcal{E}_k} \subset \Omega_i$ with $\partial\widehat{\mathcal{R}}_{\mathcal{E}_k} \cap \partial\Omega_i = \mathcal{E}_k$. For each, we construct a function $\boldsymbol{N}_{\mathcal{E}_k}$ as in Lemma 3.11. We may then use Lemma 3.11 for each $\mathcal{E}_k$. By using arguments similar to those of Lemma 3.5, we find that the support of any of these functions will intersect only a fixed number of the supports of other elments in this set of functions. Defining $\boldsymbol{N}_{\mathcal{E}d} := \sum_{k=1}^{M} \boldsymbol{N}_{\mathcal{E}_k}$, with M of order $\chi_{\mathcal{E}}(d)(d_{\mathcal{E}}/d)$, the lemma then follows from Lemma 3.11. ∎

The following Helmholtz-type decomposition and estimates allow us to make use of and build on existing tools for scalar functions in $H(\mathrm{grad}, \mathcal{D})$. We refer the reader to Lemma 5.1 of [11] for the case of polyhedral subdomains; this important paper was preceeded by [10], which concerns other applications of the same decomposition.

LEMMA 3.14. *Given a uniform domain $\mathcal{D}$ of diameter d and $\boldsymbol{u}_h \in W^{h_i}_{curl}$, there exists $p_h \in W^{h_i}_{grad}$ and $\boldsymbol{r}_h \in W^{h_i}_{curl}$ such that*

$$\boldsymbol{u}_h = \nabla p_h + \boldsymbol{r}_h, \tag{3.22}$$

$$\|\nabla p_h\|^2_{L^2(\mathcal{D})} \leq C\left(\|\boldsymbol{u}_h\|^2_{L^2(\mathcal{D})} + d^2\|\nabla \times \boldsymbol{u}_h\|^2_{L^2(\mathcal{D})}\right), \tag{3.23}$$

$$\|\boldsymbol{r}_h\|^2_{L^\infty(\mathcal{D})} \leq C(1+\log(d/h_i))\|\nabla \times \boldsymbol{u}_h\|^2_{L^2(\mathcal{D})}. \tag{3.24}$$

Proof. We can follow [11] quite closely and note that the following result is established in Lemma 5.1 of that paper: For any $\boldsymbol{u}_h \in W^{h_i}_{\mathrm{curl}}$, there exist $\boldsymbol{\Psi}_h \in (W^{h_i}_{\mathrm{grad}})^2$, $p_h \in W^{h_i}_{\mathrm{grad}}$, and $q_h \in W^{h_i}_{\mathrm{curl}}$, such that

$$\boldsymbol{u}_h = \boldsymbol{q}_h + \Pi^{h_i}(\boldsymbol{\Psi}_h) + \nabla p_h, \tag{3.25}$$

$$\|\nabla p_h\|^2_{L^2(\mathcal{D})} \leq C\left(\|\boldsymbol{u}_h\|_{L^2(\mathcal{D})} + d^2\|\nabla \times \boldsymbol{u}_h\|^2_{L^2(\mathcal{D})}\right), \tag{3.26}$$

$$\|h^{-1}\boldsymbol{q}_h\|^2_{L^2(\mathcal{D})} + \|\boldsymbol{\Psi}_h\|^2_{H(\mathrm{grad},\mathcal{D})} \leq C\|\nabla \times \boldsymbol{u}_h\|^2_{L^2(\mathcal{D})}. \tag{3.27}$$

Here, h is a piecewise constant function on the mesh $\mathcal{T}_{h_i}$ and defined by the diameter of the individual elements.

This result, in turn, is based on a stable decomposition of any $\boldsymbol{u} \in H(\mathrm{curl}, \mathcal{D})$ into a sum of two terms $\boldsymbol{\Psi} + \nabla p$, with $\boldsymbol{\Psi} \in H(\mathrm{grad}, \mathcal{D})^2$ and $p \in H(\mathrm{grad}, \mathcal{D})$, and on the finite element interpolation procedure of [18].

Such a decomposition can be derived for any John domain, and therefore also for any uniform domain, by using the main result of [1] and a simple rotation of the coordinate system, which turns the divergence operator into the curl operator.

Returning to (3.25) and defining $\boldsymbol{r}_h := \boldsymbol{q}_h + \Pi^{h_i}(\boldsymbol{\Psi}_h)$, the first estimate of the lemma follows directly from (3.26). The second estimate follows from elementary finite element estimates for $\boldsymbol{q}_h$, a simple variant of the discrete Sobolev inequality in (3.13) for $\boldsymbol{\Psi}_h$, and (3.27). ∎

4. Coarse space analysis. We define $\hat{d}_i := \max(h_i, \sqrt{\alpha_i/\beta_i})$, and consider the two cases $d_{\mathcal{E}} \leq \hat{d}_i$ (curl-dominated) and $d_{\mathcal{E}} > \hat{d}_i$ (mass-dominated). Accordingly, we partition the set of subdomain edges for Ω_i as

$$\mathcal{S}_{\mathcal{E}_i} = \mathcal{S}^c_{\mathcal{E}_i} \cup \mathcal{S}^m_{\mathcal{E}_i}$$

where for all the edges in $\mathcal{S}^c_{\mathcal{E}_i}$ we have $d_{\mathcal{E}} \leq \hat{d}_i$ and those in $\mathcal{S}^m_{\mathcal{E}_i}$ we have $d_{\mathcal{E}} > \hat{d}_i$.

We know from Lemma 3.5 there exists a uniform domain $\widehat{\mathcal{R}}_{\mathcal{E}}$ with $\partial\widehat{\mathcal{R}}_{\mathcal{E}} \cap \partial\Omega_i = \mathcal{E}$ for each $\mathcal{E} \in \mathcal{S}_{\mathcal{E}_i}$. We may thus apply Lemma 3.14 for $\widehat{\mathcal{R}}_{\mathcal{E}}$, and let $\nabla p_h + \boldsymbol{r}_h$ denote the

decomposition of $\boldsymbol{u}$ for $\widehat{\mathcal{R}}_{\mathcal{E}}$. We set $d = \hat{d}_i$ in Lemma 3.13 for the mass-dominated case and recall from the proof of Lemma 3.13 that each edge $\mathcal{E} \in \mathcal{S}^m_{\mathcal{E}_i}$ may be expressed as the union of segments $\mathcal{E}_1, \ldots, \mathcal{E}_{M(\mathcal{E},\hat{d}_i)}$. We note, by construction, that $\hat{d}_i \le d_{\mathcal{E}_k} \le 2\hat{d}_i$. Recalling the function $f^{\mathcal{E}\Delta} \in W^{h_i}_{\text{grad}}$ of Lemma 3.8 and $\boldsymbol{v}^{\mathcal{E}} \in W^{h_i}_{\text{curl}}$ of Lemma 3.12, we define

$$\boldsymbol{g} := \boldsymbol{u} - \sum_{\mathcal{E}\in\mathcal{S}_{\mathcal{E}_i}} \boldsymbol{w}^{\mathcal{E}}, \tag{4.1}$$

where

$$\boldsymbol{w}^{\mathcal{E}} = \begin{cases} \nabla p_h^{\mathcal{E}\Delta} + \boldsymbol{r}_h^{\mathcal{E}} - \bar{r}_{h\mathcal{E}} \boldsymbol{N}_{\mathcal{E}} & \text{if } \mathcal{E} \in \mathcal{S}^c_{\mathcal{E}_i}, \\ \sum_{k=1}^{M(\mathcal{E},\hat{d}_i)} \boldsymbol{u}^{\mathcal{E}_k} - \bar{u}_{\mathcal{E}} \boldsymbol{N}_{\mathcal{E}\hat{d}_i} & \text{if } \mathcal{E} \in \mathcal{S}^m_{\mathcal{E}_i}. \end{cases}$$

For each $\mathcal{E} \in \mathcal{S}^c_{\mathcal{E}_i}$, we have

$$\boldsymbol{g}\cdot\boldsymbol{t}_i = (\boldsymbol{u} - \nabla p_h - \boldsymbol{r}_h)\cdot\boldsymbol{t}_i + \left(\frac{p_h(\boldsymbol{b}) - p_h(\boldsymbol{a})}{d_{\mathcal{E}}} + \bar{r}_{h\mathcal{E}}\right)\boldsymbol{d}_{\mathcal{E}}\cdot\boldsymbol{t}_i,$$

where $\boldsymbol{a}$ and $\boldsymbol{b}$ are the endpoints of $\mathcal{E}$. The first term vanishes while the second equals $\bar{u}_{\mathcal{E}}\boldsymbol{d}_{\mathcal{E}}\cdot\boldsymbol{t}_i$. Thus, $\boldsymbol{g}\cdot\boldsymbol{t}_i = \boldsymbol{u}_0\cdot\boldsymbol{t}_i$ along $\mathcal{E}$ and the tangential data of $\boldsymbol{g}$ matches that of the coarse interpolant along $\mathcal{E} \in \mathcal{S}^c_{\mathcal{E}_i}$.

For each $\mathcal{E} \in \mathcal{S}^m_{\mathcal{E}_i}$, we have

$$\boldsymbol{g}\cdot\boldsymbol{t}_i = \left(\boldsymbol{u} - \sum_{k=1}^{M(\mathcal{E},\hat{d}_i)} \boldsymbol{u}^{\mathcal{E}_k}\right)\cdot\boldsymbol{t}_i + \bar{u}_{\mathcal{E}}\boldsymbol{d}_{\mathcal{E}}\cdot\boldsymbol{t}_i.$$

Again, the first term vanishes and $\boldsymbol{g}\cdot\boldsymbol{t}_i = \boldsymbol{u}_0\cdot\boldsymbol{t}_i$ along $\mathcal{E}$. In summary, we find that the tangential data of $\boldsymbol{g}$ along $\partial\Omega_i$ is identical to that of the coarse interpolant $\boldsymbol{u}_0$. Accordingly, we may establish energy estimates for $\boldsymbol{u}_0$ from those for $\boldsymbol{g}$ since $\boldsymbol{u}_0$ minimizes energy for the specified boundary data.

Since $d_{\mathcal{E}} \le \hat{d}_i$ for all $\mathcal{E} \in \mathcal{S}^c_{\mathcal{E}_i}$, we find from Lemmas 3.8 and 3.14 that

$$E_i(\nabla p_h^{\mathcal{E}\Delta}) \le C(1 + \log(d_{\mathcal{E}}/h_i))^2 E_{\widehat{\mathcal{R}}_{\mathcal{E}}}(\boldsymbol{u}),$$

where

$$E_{\widehat{\mathcal{R}}_{\mathcal{E}}} := \alpha_i \|\nabla\times\boldsymbol{u}\|^2_{L^2(\widehat{\mathcal{R}}_{\mathcal{E}})} + \beta_i \|\boldsymbol{u}\|^2_{L^2(\widehat{\mathcal{R}}_{\mathcal{E}})}.$$

Similarly, from Lemmas 3.12 and 3.14, we find

$$E_i(\boldsymbol{r}_h^{\mathcal{E}}) \le C(1 + \log(d_{\mathcal{E}}/h_i))^2 E_{\widehat{\mathcal{R}}_{\mathcal{E}}}(\boldsymbol{u}).$$

Next, from Lemmas 3.10, 3.14, and 3.11, we also find

$$E_i(\bar{r}_{h\mathcal{E}}\boldsymbol{N}_{\mathcal{E}}) \le C(1 + \log(d_{\mathcal{E}}/h_i))^2 E_{\widehat{\mathcal{R}}_{\mathcal{E}}}(\boldsymbol{u}).$$

In summary, we have from the previous three estimates that

$$E_i(\boldsymbol{w}^{\mathcal{E}}) \le C(1 + \log(d_{\mathcal{E}}/h_i))^2 E_{\widehat{\mathcal{R}}_{\mathcal{E}}}(\boldsymbol{u}) \quad \text{for } \mathcal{E} \in \mathcal{S}^c_{\mathcal{E}_i}. \tag{4.2}$$

We find from Lemmas 3.10 and 3.14 that

$$\left| \int_{\mathcal{E}_k} \boldsymbol{u} \cdot \boldsymbol{t}_i \, dx \right|^2 \leq C \hat{d}_i^2 (1 + \log(\hat{d}_i/h_i)) \|\nabla \times \boldsymbol{u}\|^2_{L^2(\widehat{\mathcal{R}}_{\mathcal{E}_k})},$$

and since $M(\mathcal{E}, \hat{d}_i)$ is of order $\chi_{\mathcal{E}}(\hat{d}_i)(d_{\mathcal{E}}/\hat{d}_i)$, we obtain

$$\bar{u}^2_{\mathcal{E}} \leq C \chi_{\mathcal{E}}(\hat{d}_i)(\hat{d}_i/d_{\mathcal{E}})(1 + \log(\hat{d}_i/h_i)) \|\nabla \times \boldsymbol{u}\|^2_{L^2(\widetilde{\mathcal{R}}_{\mathcal{E}})},$$

where $\widetilde{\mathcal{R}}_{\mathcal{E}} = \cup_k \widehat{\mathcal{R}}_{\mathcal{E}_k}$. It now follows from Lemma 3.13 and the definition of $\hat{d}_i$ that

$$E_i(\bar{u}_{\mathcal{E}} \boldsymbol{N}_{\mathcal{E}\hat{d}_i}) \leq C \chi^2_{\mathcal{E}}(\hat{d}_i)(1 + \log(\hat{d}_i/h_i))^2 E_{\widetilde{\mathcal{R}}_{\mathcal{E}}}(\boldsymbol{u}).$$

Similarly, it follows from Lemmas 3.12 and 3.14 that

$$E_i(\boldsymbol{u}^{\mathcal{E}_k}) \leq C(1 + \log(\hat{d}_i/h_i))^2 E_{\mathcal{R}_{\mathcal{E}_k}}(\boldsymbol{u}),$$

Since each $\widehat{\mathcal{R}}_{\mathcal{E}_k}$ only intersects a bounded number of other such regions, it follows from the previous two estimates that

$$E_i(\boldsymbol{w}^{\mathcal{E}}) \leq C \chi^2_{\mathcal{E}}(\hat{d}_i)(1 + \log(\hat{d}_i/d_{\mathcal{E}}))^2 E_{\widetilde{\mathcal{R}}_{\mathcal{E}}}(\boldsymbol{u}) \quad \text{for } \mathcal{E} \in \mathcal{S}^m_{\mathcal{E}_i}. \tag{4.3}$$

Since each $\widehat{\mathcal{R}}_{\mathcal{E}}$ and $\widetilde{\mathcal{R}}_{\mathcal{E}}$ intersects only a bounded number of other such regions, it follows from (4.2) and (4.3) that

$$E_i(\boldsymbol{u}_0) \leq E_i(\boldsymbol{g}) \leq C \chi_i^2 (1 + \log(H_i/h_i))^2 E_i(\boldsymbol{u}). \tag{4.4}$$

where $\chi_i := \max_{\mathcal{E} \in \mathcal{S}^m_{\mathcal{E}_i}} \chi_{\mathcal{E}}(\hat{d}_i)$.

5. Local decomposition. In this section, we establish estimates for an edge decomposition of the remainder obtained from subtracting the coarse interpolant $\boldsymbol{u}_0$ from $\boldsymbol{u}$. We find from (4.1) that

$$\begin{aligned} \boldsymbol{w} &:= \boldsymbol{u} - \boldsymbol{u}_0 = (\boldsymbol{g} - \boldsymbol{u}_0) + (\boldsymbol{u} - \boldsymbol{g}), \\ &= \boldsymbol{w}_{ir} + \sum_{\mathcal{E} \in \mathcal{S}_{\mathcal{E}_i}} \boldsymbol{w}^{\mathcal{E}}. \end{aligned}$$

where $\boldsymbol{w}_{ir} := \boldsymbol{g} - \boldsymbol{u}_0$ and $\boldsymbol{w}_{ir} \cdot \boldsymbol{t}_i$ vanishes on $\partial\Omega_i$. From (4.4) we have

$$E_i(\boldsymbol{w}_{ir}) \leq C \chi_i^2 (1 + \log(H_i/h_i))^2 E_i(\boldsymbol{u}). \tag{5.1}$$

We have also established estimates for the energy of $\boldsymbol{w}^{\mathcal{E}}$ in (4.2) and (4.3). We note that $\boldsymbol{w}^{\mathcal{E}} \cdot \boldsymbol{t}_i$ vanishes everywhere on $\partial\Omega_i$ except along $\mathcal{E}$.

6. Algorithm and Schwarz analysis. Before providing some implementaion details of the algorithm, we show how our iterative substructuring algorithm can be defined in terms of its local and global spaces. With reference to (2.3), we define local spaces $\boldsymbol{X}^i$ and $\boldsymbol{X}^{\mathcal{E}}$ as

$$\begin{aligned} \boldsymbol{X}^i &:= \{\boldsymbol{x} : \boldsymbol{x} = \sum_{e \in \mathcal{M}_I^{h_i}} a_e \boldsymbol{N}_e^{h_i}\}, \\ \boldsymbol{X}^{\mathcal{E}} &:= \{\boldsymbol{x} : \boldsymbol{x} = \sum_{e \in \mathcal{M}_{\mathcal{E}}} a_e \boldsymbol{N}_e^{h_i}\}, \end{aligned}$$

where $\mathcal{M}_I^{h_i}$ is the set of edges in the interior of Ω_i and $\mathcal{M}_\mathcal{E}$ is the set of edges of $\mathcal{E}$ together with those in the interiors of the two subdomains having $\mathcal{E}$ in common. With reference to (2.2), we also define the coarse space $\boldsymbol{X}^0$ as

$$\boldsymbol{X}^0 := \{\boldsymbol{x} : \boldsymbol{x} = \sum_{\mathcal{E}\in\mathcal{S}_\mathcal{E}} a_\mathcal{E}\boldsymbol{c}_\mathcal{E}\}.$$

For $\boldsymbol{u}_0 \in \boldsymbol{X}^0$, $\boldsymbol{w}^\mathcal{E} \in \boldsymbol{X}^\mathcal{E}$, and $\boldsymbol{w}_{ir} \in \boldsymbol{X}^i$, we have

$$\boldsymbol{u} = \boldsymbol{u}_0 + \sum_{\mathcal{E}\in\mathcal{S}_\mathcal{E}} \boldsymbol{w}^\mathcal{E} + \sum_{i=1}^N \boldsymbol{w}_{ir}.$$

Since each subdomain edge is common to only two subdomains and each of the regions $\widetilde{\mathcal{R}}_\mathcal{E}$ and $\widehat{\mathcal{R}}_\mathcal{E}$ intersects only a bounded number of other such regions, we find from (4.2), (4.3), and (4.4) that

$$\begin{aligned}
\sum_{i=1}^N E_i(\boldsymbol{u}_0) &\le C\omega^2 \sum_{i=1}^N E_i(\boldsymbol{u}),\\
\sum_{i=1}^N \sum_{\mathcal{E}\in\mathcal{S}_{\mathcal{E}_i}} E_i(\boldsymbol{w}^\mathcal{E}) &\le C\omega^2 \sum_{i=1}^N E_i(\boldsymbol{u}),\\
\sum_{i=1}^N \sum_{j=1}^N E_i(\boldsymbol{w}_{jr}) &\le C\omega^2 \sum_{i=1}^N E_i(\boldsymbol{u}),
\end{aligned}$$

where

$$\omega := \max_i \chi_i(1 + \log(H_i/h_i)).$$

We have thus shown

$$C_0^2 \le C\omega^2,$$

where C_0 is the constant for the stable decomposition of $\boldsymbol{u}$ in [24, Assumption 2.2]. We note that C does not depend on possible jumps in coefficients between subdomains nor on the maximum number of edges for any subdomain. In addition, the maximum ratio of edge lengths for any subdomain may grow with mesh refinement without increasing C. From Lemma 2.5 of [24] we find that the smallest eigenvalue of the Schwarz operator P_{ad} is bounded below by C_0^{-2}. Thus,

$$1/\lambda_{\min}(P_{ad}) \le C\omega^2. \tag{6.1}$$

Since our algorithm uses exact local solvers, we find from from Lemmas 2.6 and 2.10 of [24] that

$$\lambda_{\max}(P_{ad}) \le N^c + 1, \tag{6.2}$$

where N^c is the minimum number of colors needed to color the subdomains. Since the local space for each subdomain edge extends into the interiors of both subdomains sharing the edge, no two edges can have the same color if they are part of the same subdomain. This implies the bound for $\lambda_{\max}(P_{ad})$ grows linearly with the maximum

number of edges for any subdomain. This observation is confirmed numerically in the final example of the next section.

Our main result now follows from the estimates in (6.1) and (6.2).

THEOREM 6.1. *The condition number $\kappa(P_{ad})$ of the Schwarz operator for our iterative substructuring algorithm is bounded above by the estimate*

$$\kappa(P_{ad}) := \lambda_{\max}(P_{ad})/\lambda_{\min}(P_{ad}) \leq C(1+N^c)\omega^2.$$

Comparing the estimate in Theorem 6.1 with (1.1), we see that the factor of $\max_i H_i^2\beta_i/\alpha_i$ is no longer present. In addition, the estimate applies to a much broader class of subdomain shapes.

6.1. Implementation Details. When solving a linear system $Kx = f$ for the discretized problem, we must apply a preconditioner M^{-1} to the current residual vector r in each conjugate gradient iteration. In this subsection, we provide some details on calculating $M^{-1}r$ for both the iterative substructuring algorithm of this study and for an overlapping Schwarz approach which uses the same coarse space.

Let the Boolean matrices R_I and R_Γ select the rows of x corresponding to edges in subdomain interiors and on the interface Γ, respectively. For iterative substructuring methods, the conjugate gradient algorithm is used to solve the interface problem $Sx_\Gamma = g$, where $S = K_{\Gamma\Gamma} - K_{\Gamma I}K_{II}^{-1}K_{I\Gamma}$, $x_\Gamma = R_\Gamma x$, $g = f_\Gamma - K_{\Gamma I}K_{II}^{-1}f_I$,

$$f_I = R_I f, \quad f_\Gamma = R_\Gamma f, \quad K_{II} = R_I K R_I^T, \quad K_{I\Gamma} = R_I K R_\Gamma^T, \quad \text{etc.}$$

We note that the Schur complement matrix S needs not be formed explicitly in order to calculate products of the form Sx_Γ required by the conjugate gradient algorithm. We also note that once x_Γ is obtained, x_I can be recovered from $x_I = K_{II}^{-1}(f_I - K_{I\Gamma}x_\Gamma)$.

Each column m of the coarse matrix Φ_Γ is associated with a specific subdomain edge $\mathcal{E}_m$. Let $\boldsymbol{t}_{e_k}$ denote the unit tangent vector for the edge associated with row k of x_Γ. The entry in row k and column m of Φ_Γ is given by $\delta_{km}\boldsymbol{t}_{e_k}\cdot\boldsymbol{d}_{\mathcal{E}_m}$, where $\delta_{km} = 1$ if $e_k \subset \mathcal{E}_m$ and $\delta_{km} = 0$ otherwise. The coarse matrix for the problem is then given by

$$K_c = \Phi_\Gamma^T S \Phi_\Gamma.$$

We next introduce three more Boolean matrices for bookkeeping purposes. Let $R_{1\mathcal{E}}$ select the rows of x corresponding to edges in the interior of the two subdomains sharing $\mathcal{E}$ together with those for $\mathcal{E}$ itself. Next, let $R_{2\mathcal{E}}$ select the rows of $R_{1\mathcal{E}}x$ corresponding to the edges of $\mathcal{E}$. Finally, let $R_{3\mathcal{E}}$ select the rows of x_Γ corresponding to edges of $\mathcal{E}$. We note that $R_{2\mathcal{E}}R_{1\mathcal{E}}x = R_{3\mathcal{E}}x_\Gamma$.

Given a residual vector r, the preconditioned residual for the two-level additive Schwarz algorithm is given by

$$M^{-1}r = \Phi_\Gamma K_c^{-1}\Phi_\Gamma^T r + \sum_{\mathcal{E}\in\mathcal{S}_\mathcal{E}} R_{3\mathcal{E}}^T R_{2\mathcal{E}}(R_{1E}KR_{1E}^T)^{-1}R_{2\mathcal{E}}^T R_{3\mathcal{E}}r.$$

Other variants of the preconditioner such as with a multiplicative coarse space correction are also possible; cf. [24, Section 2.5.2].

For the overlapping Schwarz algorithm, let R_i select the rows of x corresponding to an overlapping subdomain Ω_i'. Typically, Ω_i' is obtained by extending Ω_i by an integer number of layers of elements. The preconditioned residual in this case is given

by

$$M^{-1}r = \Phi K_c^{-1}\Phi^T + \sum_{i=1}^{N} R_i^T (R_i K R_i^T)^{-1} R_i r,$$

where

$$\Phi = R_\Gamma^T \Phi_\Gamma - R_I^T K_{II}^{-1} K_{I\Gamma} \Phi_\Gamma.$$

We note that in a parallel computing setting, the construction of Φ along with the local contributions to the preconditioned residual can be calculated concurrently. The coarse corrections in either algorithm, however, cannot in general be done in parallel. Finally, we note if the coarse matrix K_c becomes too large to factor with a direct method, then it is possible to obtain an approximate coarse solution by applying the iterative substructuring or overlapping Schwarz preconditioner to the coarse problem itself.

7. Numerical examples. Numerical examples are presented in this section to confirm the theory for both regular and irregular-shaped subdomains. For the first three examples, we consider three different types of subdomains. Type 1 subdomains have a square geometry and consist of square edge elements. Type 2 subdomains also consist of square edge elements, but the subdomain edges have ragged shapes which are not uniformly Lipschitz continuous. Finally, Type 3 subdomains contain equilateral triangular edge elements, and have subdomain edges with both straight-line and pre-fractal segments. A more detailed description of these three subdomain types along with accompanying pictures can be found in [5].

In addition to the classical iterative substructuring (CIS) algorithm analyzed here, we also present numerical results for an overlapping Schwarz (OS) algorithm which uses the same coarse space. This is done for purposes of comparison; the analysis of an overlapping Schwarz algorithm will appear in a forthcoming study for 3D problems. The method of preconditioned conjugate gradients is used to solve linear systems with random right-hand sides to a relative residual tolerance of 10^{-8}. The numbers of iterations and condition number estimates (in parenthesis) of the conjugate gradient iterations are reported in each of the tables. The dimensionless parameter H/δ denotes the relative overlap for the overlapping Schwarz algorithm; cf. [5].

7.1. Example 1. This example is used to confirm that the condition number estimate for the Schwarz operator is independent of the number of subdomains. The scalability of both the CIS and OS algorithms is evident in Table 7.1.

7.2. Example 2. This example is used to confirm the polylogarithmic condition number estimate in Theorem 6.1. The results in Table 7.2 for the CIS algorithm are plotted in Fig. 7.1 for $\beta = 10^{-3}$, and are consistent with theory. In addition to being noticeably smaller, the condition number estimates in Table 7.2 for the OS algorithm are much less sensitive to the mesh parameter H/h.

7.3. Example 3. This example is used to confirm that the estimate in Theorem 6.1 is independent of the material property values in each subdomain. We note that insensitivity to jumps in material properties is evident in Table 7.3 for both domain decomposition algorithms.

TABLE 7.1

Results for unit square domain decomposed into N subdomains, each with $H/h = 4$. Numbers of iterations and condition number estimates (in parenthesis) are reported for a relative residual tolerance of 10^{-8}. Subdomain material properties given by $\alpha_i = 1$ and $\beta_i = \beta$.

		classical iterative substructuring			overlapping Schwarz ($H/\delta = 4$)		
Type	N	$\beta = 10^{-3}$	$\beta = 1$	$\beta = 10^{3}$	$\beta = 10^{-3}$	$\beta = 1$	$\beta = 10^{3}$
1	16	18(16.7)	15(16.3)	8(3.8)	14(5.1)	12(5.0)	8(4.6)
	64	25(18.6)	21(18.3)	10(6.1)	13(5.2)	12(5.2)	9(4.5)
	144	28(19.1)	22(18.9)	12(8.1)	13(5.1)	12(5.1)	10(4.6)
	256	30(19.4)	23(19.0)	14(9.9)	12(5.1)	12(5.1)	10(4.7)
	400	30(19.5)	25(19.3)	15(11.6)	12(5.0)	12(5.0)	10(4.7)
	576	30(19.5)	25(19.3)	16(12.7)	12(5.0)	12(5.0)	11(4.8)
	784	30(19.5)	25(19.3)	16(13.7)	12(5.0)	12(5.0)	11(4.8)
	1024	30(19.5)	25(19.3)	17(14.5)	12(5.0)	12(5.0)	11(4.8)
2	16	26(30.0)	20(28.5)	8(3.7)	14(5.0)	12(4.8)	8(4.6)
	64	36(33.6)	29(33.0)	11(6.8)	17(6.9)	14(7.0)	9(4.5)
	144	40(34.2)	31(33.8)	14(10.0)	19(7.6)	15(7.6)	10(4.5)
	256	42(34.5)	33(34.1)	17(13.1)	19(7.5)	15(7.5)	10(4.5)
	400	43(34.6)	34(34.3)	18(15.8)	20(8.0)	16(7.9)	10(4.5)
	576	43(34.7)	34(34.3)	20(18.5)	20(8.0)	16(8.0)	11(4.6)
	784	44(34.8)	35(34.6)	21(20.8)	20(7.9)	16(7.9)	11(4.6)
	1024	44(34.8)	36(34.6)	22(22.6)	20(8.1)	17(8.2)	11(5.0)

TABLE 7.2

Results for unit square domain decomposed into 16 subdomains; the domain is triangular for Type 3 subdomains. Subdomain material properties given by $\alpha_i = 1$ and $\beta_i = \beta$.

		classical iterative substructuring			overlapping Schwarz ($H/\delta = 4$)		
Type	H/h	$\beta = 10^{-3}$	$\beta = 1$	$\beta = 10^{3}$	$\beta = 10^{-3}$	$\beta = 1$	$\beta = 10^{3}$
1	4	18(16.7)	15(16.3)	8(3.8)	14(5.1)	12(5.0)	8(4.6)
	8	20(23.7)	17(23.3)	9(5.8)	12(5.1)	12(5.1)	8(4.6)
	16	23(32.1)	18(31.4)	10(8.5)	13(5.1)	12(4.9)	9(4.5)
	32	26(42.0)	19(41.0)	11(12.4)	13(5.0)	12(4.8)	9(4.5)
2	4	26(30.0)	20(28.5)	8(3.7)	14(5.0)	12(4.8)	8(4.6)
	8	27(39.3)	21(37.8)	10(6.2)	14(4.5)	11(4.4)	9(4.5)
	16	24(49.8)	19(48.3)	11(11.0)	13(4.6)	11(4.3)	9(4.5)
	32	26(60.6)	22(59.0)	14(18.0)	13(4.8)	12(4.6)	9(4.5)
3	15	20(44.8)	19(44.5)	13(13.2)	17(8.3)	15(8.2)	11(6.3)
	45	24(71.0)	21(70.5)	12(25.3)	17(7.9)	15(7.9)	12(6.3)
	135	29(104)	26(103)	17(42.7)	17(8.1)	16(8.1)	13(6.3)

TABLE 7.3

Classical iterative substructuring (CIS) and overlapping Schwarz (OS) results for unit square domain decomposed into 64 subdomains, each with $H/h = 8$ and $H/\delta = 4$ for OS. The eight subdomains along the diagonal from $(0,0)$ to $(1,1)$ have $\alpha_i = \alpha$ and $\beta_i = \beta$, while the remaining subdomains have $\alpha_i = 1$ and $\beta_i = 1$.

		Type 1		Type 2	
α	β	CIS	OS	CIS	OS
10^{-3}	10^{-3}	25(26.2)	14(5.7)	35(46.7)	15(6.6)
10^{-3}	1	24(26.0)	13(5.1)	34(43.8)	13(5.4)
10^{-3}	10^{3}	21(25.1)	13(5.5)	33(43.2)	15(9.8)
1	10^{-3}	26(26.3)	13(6.5)	36(46.7)	15(8.0)
1	1	24(26.3)	12(5.1)	32(44.5)	13(5.4)
1	10^{3}	24(24.7)	12(5.2)	32(41.9)	13(5.6)
10^{3}	10^{-3}	31(27.3)	13(6.4)	40(48.7)	15(7.9)
10^{3}	1	25(27.2)	12(5.1)	34(46.2)	13(5.4)
10^{3}	10^{3}	26(26.8)	14(6.4)	34(47.2)	15(6.8)

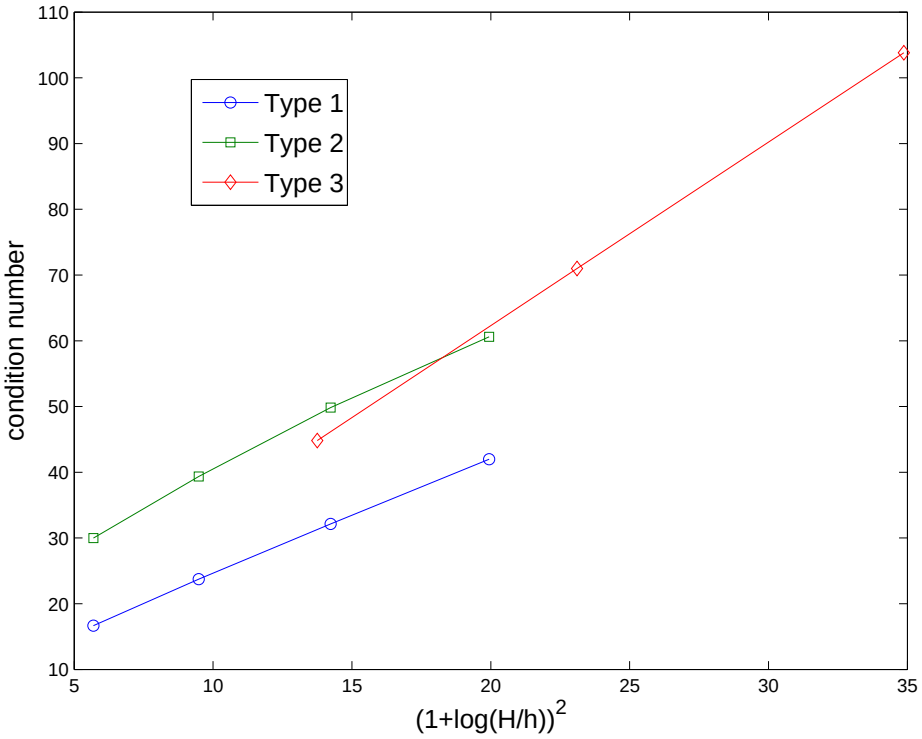

FIG. 7.1. *Plot of classical iterative substructuring data in Table 7.2 confirming the theoretical estimate in Theorem 6.1.*

7.4. Example 4. This example is used to demonstrate that the performance of the CIS and OS algorithms need not be diminished significantly when a mesh partitioner is used to decompose the mesh. Example mesh decompositions for $N = 16$ and $N = 64$, shown in Fig. 7.2, were obtained using the graph partitioning software Metis [14] as described in [5]. The results in Table 7.4 show that iteration counts and condition number estimates do not grow dramatically when switching from square subdomains to ones obtained from the mesh partitioner.

7.5. Example 5. This example is used to confirm that our condition number estimate does not require all subdomain edges to be of comparable length. Here, the smaller square subdomains shown in Fig. 7.3 always have 4 elements while the mesh parameter H/h is increased for the larger surrounding subdomains. The condition number estimates shown in Table 7.5 for the CIS algorithm are consistent with our theory.

7.6. Example 6. The final example is used to confirm the estimates in (6.1) and (6.2). Here we have two large subdomains and smaller square subdomains with centers along $x = 1/2$, and whose number grows with mesh refinement (see Fig. 7.4). Thus, the number of subdomain edges for the two larger subdomains grows linearly with H/h. The results in Table 7.6 are consistent with the theoretical estimates. We also note that the results for the overlapping Schwarz algorithm are much less sensitive to increasing numbers of subdomain edges; this can easily be established by a coloring argument.

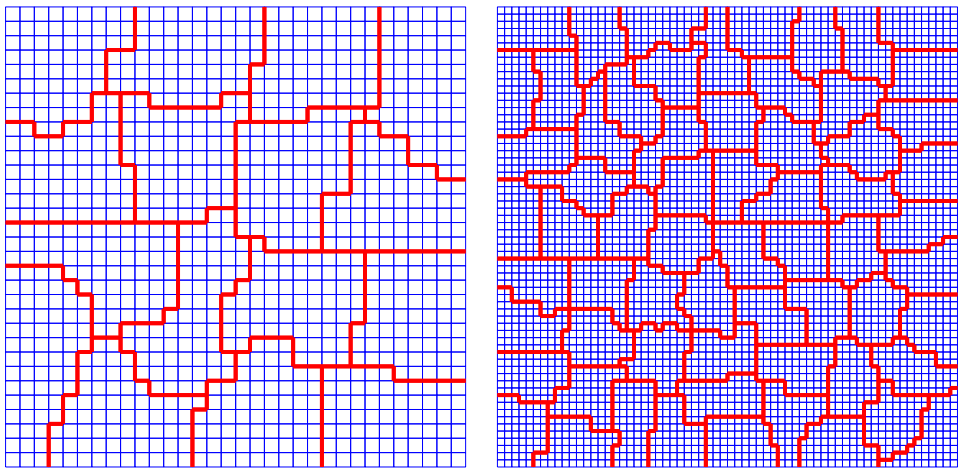

FIG. 7.2. *Example decompositions ($N = 16$ and $N = 64$) used in Example 7.4*

TABLE 7.4

Results for unit square domain decomposed into N subdomains. There are 64 elements per subdomain for the Type 1 (square) subdomains and approximately 64 elements per subdomain for subdomains obtained from the mesh partitioner. Material properties are homogeneous with $\alpha_i = 1$ and $\beta_i = \beta$.

		classical iterative substructuring			overlapping Schwarz ($H/\delta = 4$)		
Type	N	$\beta = 10^{-3}$	$\beta = 1$	$\beta = 10^3$	$\beta = 10^{-3}$	$\beta = 1$	$\beta = 10^3$
1	16	20(23.7)	17(23.3)	9(5.8)	12(5.1)	12(5.1)	8(4.6)
	64	29(26.6)	24(26.3)	12(9.2)	12(5.1)	12(5.1)	10(4.5)
	144	31(27.1)	25(26.8)	14(12.2)	12(5.1)	12(5.1)	10(4.5)
	256	34(27.4)	26(27.1)	16(14.7)	12(5.1)	11(5.0)	11(4.7)
	400	35(27.6)	26(27.3)	17(16.6)	11(5.0)	11(5.0)	11(4.7)
Metis	16	30(27.8)	23(25.4)	10(5.2)	13(6.5)	13(6.5)	9(5.0)
	64	40(33.7)	30(32.2)	13(8.8)	13(5.5)	12(5.4)	11(4.8)
	144	42(37.4)	33(36.2)	15(11.9)	18(8.0)	16(7.9)	12(5.9)
	257	45(38.6)	35(36.8)	17(13.3)	16(7.2)	16(17.1)	13(6.3)
	400	46(41.9)	36(40.8)	17(13.7)	16(7.1)	15(6.9)	13(6.1)

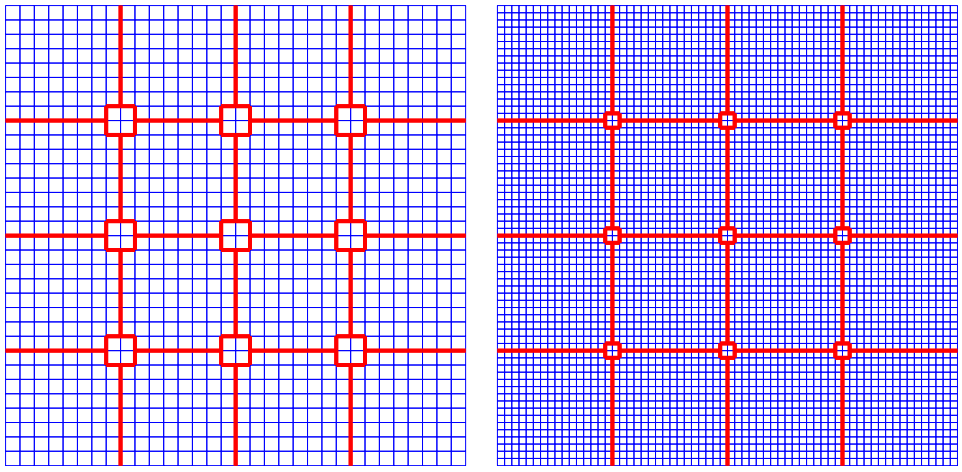

FIG. 7.3. *Example decompositions ($H/h = 8$ and $H/h = 16$) used in Example 7.5.*

TABLE 7.5

Results for Example 7.5 (see also Fig. 7.3). Material properties are homogeneous with $\alpha_i = 1$ and $\beta_i = \beta$.

	classical iterative substructuring			overlapping Schwarz ($H/\delta = 4$)		
H/h	$\beta = 10^{-3}$	$\beta = 1$	$\beta = 10^3$	$\beta = 10^{-3}$	$\beta = 1$	$\beta = 10^3$
4	23(15.3)	18(14.7)	8(3.4)	15(5.1)	12(4.9)	8(4.2)
8	25(16.5)	19(16.0)	10(5.0)	16(6.5)	13(6.3)	9(5.2)
12	25(19.2)	20(18.8)	10(6.8)	16(6.2)	14(6.1)	10(5.8)
16	27(21.4)	21(20.9)	11(8.4)	15(6.4)	14(5.9)	10(5.9)
20	28(23.1)	22(22.5)	12(9.7)	15(6.4)	14(5.9)	10(5.9)

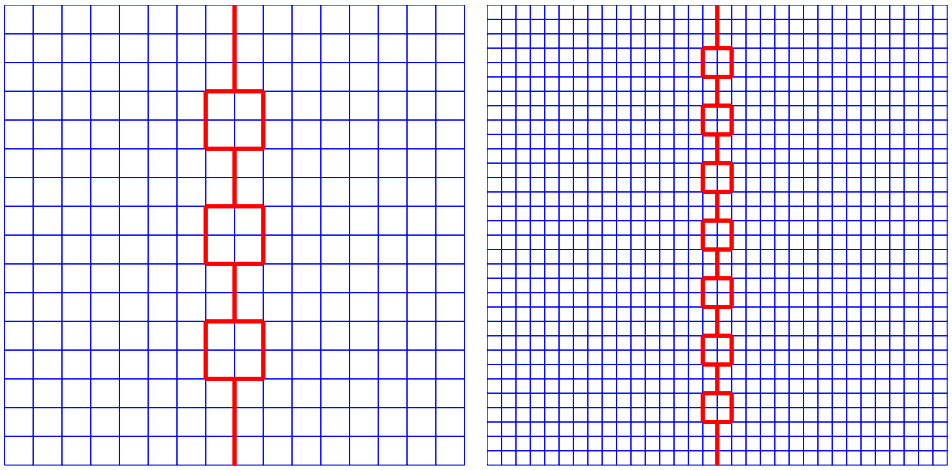

FIG. 7.4. *Example decompositions ($H/h = 8$ and $H/h = 16$) used in Example 7.6.*

REFERENCES

[1] Gabriel Acosta, Ricardo G. Durán, and María A. Muschietti. Solutions of the divergence operator on John domains. *Adv. Math.*, 206(2):373–401, 2006.

[2] Rudi Beck, Ralf Hiptmair, Ronald H. W. Hoppe, and Barbara Wohlmuth. Residual based a posteriori error estimators for eddy current computation. *M2AN Math. Model. Numer. Anal.*, 34(1):159–182, 2000.

[3] Stephen M. Buckley and Pekka Koskela. Sobolev-Poincaré implies John. *Math. Res. Lett.*, pages 577–593, 1995.

[4] Clark R. Dohrmann, Axel Klawonn, and Olof B. Widlund. A family of energy minimizing coarse spaces for overlapping Schwarz preconditioners. In Ulrich Langer, Marco Discacciati, David Keyes, Olof Widlund, and Walter Zulehner, editors, *Proceedings of the 17th International Conference on Domain Decomposition Methods in Science and Engineering, held in Strobl, Austria, July 3-7, 2006*, number 60 in Springer-Verlag, Lecture Notes in Computational Science and Engineering, pages 247–254, 2007.

[5] Clark R. Dohrmann, Axel Klawonn, and Olof B. Widlund. Domain decomposition for less regular subdomains: Overlapping Schwarz in two dimensions. *SIAM J. Numer. Anal.*, 46(4):2153–2168, 2008.

[6] Clark R. Dohrmann and Olof B. Widlund. An overlapping Schwarz algorithm for almost incompressible elasticity. *SIAM J. Numer. Anal.*, 47(4):2897–2923, 2009.

[7] Clark R. Dohrmann and Olof B. Widlund. Hybrid domain decomposition algorithms for compressible and almost incompressible elasticity. *Internat. J. Numer. Meth. Engng.*, 82:157–183, 2010.

[8] Kenneth Falconer. *Fractal Geometry: Mathematical Foundations and Applications.* John Wiley & Sons Inc., Hoboken, NJ, second edition, 2003.

[9] Ralf Hiptmair. Finite elements in computational electromagnetism. *Acta Numer.*, 11:237–339, 2002.

TABLE 7.6

Results for Example 7.6 (see also Fig. 7.4). Material properties are homogeneous with $\alpha_i = 1$ and $\beta_i = 10^{-3}$. The overlapping Schwarz results are for $H/\delta = 4$.

	CIS			OS
H/h	$\kappa(P_{ad})$	$\lambda_{\min}(P_{ad})$	$\lambda_{\max}(P_{ad})$	$\kappa(P_{ad})$
4	13.7	0.227	3.12	4.1
8	22.3	0.227	5.09	4.1
12	31.0	0.227	7.07	5.0
16	39.7	0.227	9.05	5.9
20	48.4	0.227	11.0	6.0

[10] Ralf Hiptmair, Gisela Widmer, and Jun Zou. Auxiliary space preconditioning in $H_0(\mathrm{curl};\ \Omega)$. *Numer. Math.*, 103(3):435–459, 2006.

[11] Ralf Hiptmair and Jinchao Xu. Nodal auxiliary space preconditioning in H(curl) and H(div) spaces. *SIAM J. Numer. Anal.*, 45(6):2483–2509 (electronic), 2007.

[12] Qiya Hu and Jun Zou. A nonoverlapping domain decomposition method for Maxwell's equations in three dimensions. *SIAM J. Numer. Anal.*, 41(5):1682–1708, 2003.

[13] Peter W. Jones. Quasiconformal mappings and extendability of functions in Sobolev space. *Acta Math.*, 147(1-2):71–88, 1981.

[14] George Karypis and Vipin Kumar. *METIS Version 4.0*. University of Minnesota, Department of Computer Science, Minneapolis, MN, 1998.

[15] Axel Klawonn, Oliver Rheinbach, and Olof B. Widlund. An analysis of a FETI–DP algorithm on irregular subdomains in the plane. *SIAM J. Numer. Anal.*, 46(5):2484–2504, 2008.

[16] Jean-Claude Nédélec. Mixed finite elements in R^3. *Numer. Math.*, 35:315–341, 1980.

[17] Francesca Rapetti and Andrea Toselli. A FETI preconditioner for two dimensional edge element approximations of Maxwell's equations on nonmatching grids. *SIAM J. Sci. Comput.*, 23(1):92–108, 2001.

[18] L. Ridgway Scott and Shangyou Zhang. Finite element interpolation of nonsmooth functions satisfying boundary conditions. *Math. Comp.*, 54(190):483–493, 1990.

[19] Andrea Toselli. Neumann-Neumann methods for vector field problems. *Electron. Trans. Numer. Anal.*, 11:1–24, 2000.

[20] Andrea Toselli. Overlapping Schwarz methods for Maxwell's equations in three dimensions. *Numer. Math.*, 86:733–752, 2000.

[21] Andrea Toselli. Dual–primal FETI algorithms for edge finite–element approximations in 3D. *IMA J. Numer. Anal.*, 26:96–130, 2006.

[22] Andrea Toselli and Axel Klawonn. A FETI domain decomposition method for edge element approximations in two dimensions with discontinuous coefficients. *SIAM J. Numer. Anal.*, 39(3):932–956, 2001.

[23] Andrea Toselli and Xavier Vasseur. Dual–primal FETI algorithms for edge element approximations: two–dimensional h and p finite elements on shape–regular meshes. *SIAM J. Numer. Anal.*, 42(6):2590–2611, 2005.

[24] Andrea Toselli and Olof Widlund. *Domain Decomposition Methods - Algorithms and Theory*, volume 34 of *Springer Series in Computational Mathematics*. Springer-Verlag, Berlin Heidelberg New York, 2005.

[25] Andrea Toselli, Olof B. Widlund, and Barbara I. Wohlmuth. An iterative substructuring method for Maxwell's equations in two dimensions. *Math. Comp.*, 70(235):935–949, 2000.